Type of the Paper (Article)

Necessity to use the true gravity in large scale atmospheric modeling

Peter C. Chu[1,*]

[1] Department of Oceanography, Naval Postgraduate School, Monterey, CA 93943, USA; pcchu@nps.edu
* Correspondence: pcchu@nps.edu

Abstract: Newton's law of universal gravitation applies between two point-masses. **True gravitation** of solid Earth is volume integration of gravitation of all point-masses inside the solid Earth on a point-mass in atmosphere. However, in meteorology **the Earth "shrinks" into a point-mass located at Earth center with entire Earth mass to identify the Earth gravitation (untrue)**. Combination of untrue gravitational and centrifugal accelerations gives effective gravity ($\mathbf{g}_{eff}$). Combination of true gravitational and centrifugal accelerations leads to true gravity ($\mathbf{g}$). The true gravity $\mathbf{g}$ minus the effective gravity $\mathbf{g}_{eff}$ is the gravity disturbance vector, $\delta\mathbf{g} = \mathbf{g} - \mathbf{g}_{eff}$. With the true gravity $\mathbf{g}$ used in the basic equations, seven $n$on-dimensional numbers are proposed to identify the importance of $\delta\mathbf{g}$ versus traditional forcing terms such as horizontal pressure gradient force and Coriolis force. These non-dimensional numbers are calculated from two publicly available datasets with the geoid undulation (N) from the static gravity field model EIGEN-6C4 and long-term mean geopotential height (Z), wind velocity (u, v), and temperature (T_a) at 12 pressure levels in troposphere from the NCEP/NCAR reanalyzed climatology. The results demonstrate $\delta\mathbf{g}$ nonnegligible in hydrostatic equilibrium, geostrophic wind, geostrophic vorticity, Ekman pumping, Q vector, and Omega equation, but negligible in thermal wind relation.

Keywords: true gravity; effective gravity; gravity disturbance vector; geoid undulation; gravity field mode EIGEN-6C4

1. Introduction

Every meteorologist including the author from very beginning of her/his career learned that the Earth gravity on a point-mass in atmosphere (m_A) at location $\mathbf{r}_A$ consists of Earth gravitation and centrifugal force with the Earth center ($\mathbf{O}$) as the origin of the position vector $\mathbf{r}_A$ (Figure 1). ***The solid Earth "shrinks" into a point-mass located at the Earth center with the entire Earth mass to get the Earth gravitation.*** With such a treatment, the Earth gravitation on m_A, given by $\mathbf{F}_N^{(O)}(\mathbf{r}_A)$, is between the Earth point-mass M_O (at point $\mathbf{O}$) and atmospheric point-mass m_A,

$$\mathbf{F}_N^{(O)}(\mathbf{r}_A) = -m_A \frac{GM}{|\mathbf{r}_A|^2}\frac{\mathbf{r}_A}{|\mathbf{r}_A|} = -m_A g_0 \frac{\mathbf{r}_A}{|\mathbf{r}_A|}, \quad g_0 = 9.81\ \text{m/s}^2 \tag{1}$$

where $G = 6.67408\times10^{-11}\text{Nm}^2\text{kg}^{-2}$, is the Newtonian gravitational constant; and $M = 5.98\times10^{24}$ kg is the mass of the Earth. Since $\mathbf{F}_N^{(O)}(\mathbf{r}_A)$ in Eq.(1) is calculated through shrinking the solid Earth into a point-mass M_O. It is not true and therefore should be called the untrue Earth gravitation.

Preprints (www.preprints.org) | NOT PEER-REVIEWED | Posted: 7 February 2023 doi:10.20944/preprints202302.0127.v1

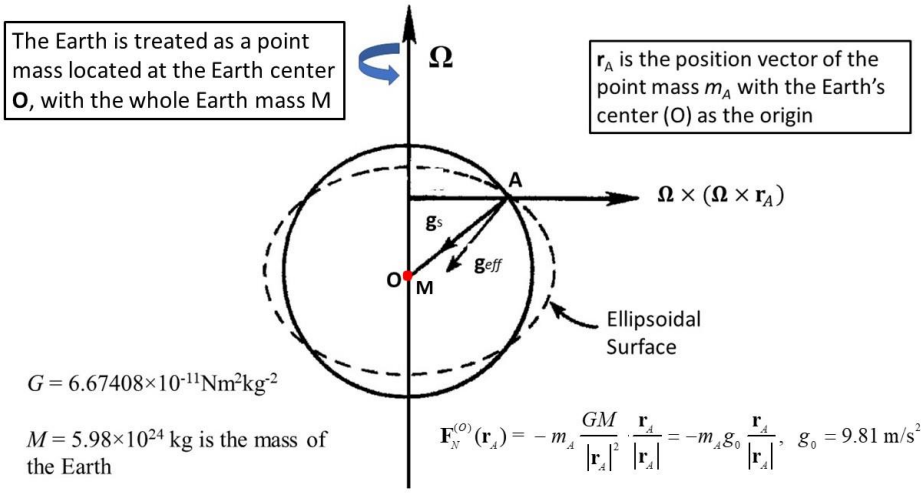

Figure 1. In dynamic meteorology, the solid Earth shrinks into a point-mass (shown as the red dot) located at the Earth center (**O**) with the entire Earth mass. The Earth gravitation (untrue) on the point-mass m_A in the atmosphere is between the point-mass M_O and point-mass m_A, and represented by $\mathbf{F}_N^{(O)}$. Combination of the untrue Earth gravitational and centrifugal accelerations leads to the effective gravity $\mathbf{g}_{eff}$ which is used in atmospheric modeling ever since.

Let $\boldsymbol{\Omega}$ be the Earth's angular velocity with $|\boldsymbol{\Omega}| = 2\pi/(86164\text{ s})$. Combining the untrue gravitation ($\mathbf{F}_N^{(O)}$) with the centrifugal force ($\mathbf{F}_C$) on the point-mass m_A

$$\mathbf{F}^{(O)}(\mathbf{r}_A) = \mathbf{F}_N^{(O)}(\mathbf{r}_A) + \mathbf{F}_C(\mathbf{r}_A) = -m_A g_0 \frac{\mathbf{r}_A}{|\mathbf{r}_A|} + m_A \boldsymbol{\Omega} \times (\boldsymbol{\Omega} \times \mathbf{r}_A) \tag{2}$$

leads to the effective gravity ($\mathbf{g}_{eff}$, sometimes called normal gravity, or apparent gravity) [1] (pp 12-14)

$$\mathbf{g}_{eff} = -g_0 \frac{\mathbf{r}_A}{|\mathbf{r}_A|} + \boldsymbol{\Omega} \times (\boldsymbol{\Omega} \times \mathbf{r}_A) \tag{3}$$

The effective gravity $\mathbf{g}_{eff}$ is non-radial (not in the direction of $\mathbf{r}_A$) but changes little with latitude or height. The rotation causes equatorial bulge and polar flattening, i.e., uniform ellipsoidal Earth. Let $\mathbf{k}$ be the unit vector perpendicular to the ellipsoidal Earth surface. The effective gravity $\mathbf{g}_{eff}$ at the Earth surface is given by (https://glossary.ametsoc.org/wiki/Gravity)

$$\mathbf{g}_{eff} = -g(\varphi)\mathbf{k}, \quad g(\varphi) = 9.806160\left(1 - 0.0026373\cos 2\varphi + 0.0000059\cos^2 2\varphi\right) \tag{4}$$

where φ is the latitude.

To solve the non-radial nature of $\mathbf{g}_{eff}$, orthogonal curvilinear coordinate systems, i.e., the geopotential coordinates (more accurately called the effective geopotential coordinates) have been used. Among them, the oblate spheroid coordinate system (λ, φ, z) with ($\mathbf{i}$, $\mathbf{j}$, $\mathbf{k}$) the corresponding unit vectors is optimal since it describes the ellipsoidal

Preprints (www.preprints.org) | NOT PEER-REVIEWED | Posted: 7 February 2023 doi:10.20944/preprints202302.0127.v1

shape more accurately. However, the error is less than 0.17% between polar spherical coordinate and oblate spherical coordinate systems [2] (P.92). The geophysically realistic, ellipsoidal, analytically tractable (GREAT) coordinates was presented [3] to make that the horizontal coordinate surfaces coincide with the effective geopotential (Φ_{eff}) surfaces and to ensure that there is no component of effective gravity ($\mathbf{g}_{eff}$) in any direction tangential to coordinate surfaces (i.e., no horizontal compoenent in $\mathbf{g}_{eff}$),

$$\mathbf{g}_{eff} = -\frac{d\Phi_{eff}}{dz}\mathbf{k} \tag{5a}$$

where the direction of $\mathbf{k}$ is defined as the vertical in meteorology. The effective geopotential Φ_{eff} is given by [2] (P.46, Equation 3.5.2) [5-6]

$$g(\varphi) = \frac{d\Phi_{eff}}{dz} \approx g_0, \quad \Phi_{eff} \approx g_0 z\,. \tag{5b}$$

where z is the height of the point mass in atmosphere with z = 0 at the Earth ellipsoidal surface. Vertical integration of (5b) from z = 0 to the height of the point mass in atmosphere (z) leads to

$$Z = \frac{1}{g_0}\int_0^z \frac{d\Phi_{eff}}{dz}\,dz' \tag{6}$$

where Z is the effective geopotential height of the point mass. The two heights (z and Z) are numerically interchangeable for most meteorological purpose (see website: https://glossary.ametsoc.org/wiki/Geopotential_height). The effective gravity $\mathbf{g}_{eff}$ with no horizontal component has been used in atmospheric dynamics and modeling as if it were the true gravity.

A question arises: ***Is it reasonable to shrink the solid Earth into a point-mass with the entir Earth mass*** *(M)* ***concentrated at the Earth center*** **(O)** ***in calculating the Earth gravitation?*** The answer is **NO** because the solid Earth contains infinite number of point-masses. The Newton's law of universal gravitation in today's language states that every point-mass attracts every other point mass by a force acting along the line intersecting the two points. The force is proportional to the product of the two point-masses, and inversely proportional to the square of the distance between them (see website https://en.wikipedia.org/wiki/Newton%27s_law_of_universal_gravitation.)

Let $\mathbf{r}$ be the position vector of a point inside the solid Earth, $\sigma(\mathbf{r})$ be the mass density, and $d\Pi$ be the infinitesimally small volume (around $\mathbf{r}$). The point-mass at $\mathbf{r}$ is represented by

$dm(\mathbf{r}) = \sigma(\mathbf{r})d\Pi$.

Preprints (www.preprints.org) | NOT PEER-REVIEWED | Posted: 7 February 2023 doi:10.20944/preprints202302.0127.v1

The Newton's gravitation of point-mass $dm(\mathbf{r})$ on a point mass m_A at location $\mathbf{r}_A$ in atmosphere is given by

$$d\mathbf{F}_N(\mathbf{r}_A) = Gm_A dm(\mathbf{r})\frac{(\mathbf{r}-\mathbf{r}_A)}{|\mathbf{r}-\mathbf{r}_A|^3} = Gm_A\sigma(\mathbf{r})\frac{(\mathbf{r}-\mathbf{r}_A)}{|\mathbf{r}-\mathbf{r}_A|^3}d\Pi \tag{7a}$$

The gravitation of the whole Earth on the point-mass m_A is the volume integration (Figure 2) [4] (P.72, Equation 6.4),

$$\mathbf{F}_N(\mathbf{r}_A) = \iiint_\Pi d\mathbf{F}_N(\mathbf{r}_A) = Gm_A\iiint_\Pi \sigma(\mathbf{r})\frac{(\mathbf{r}-\mathbf{r}_A)}{|\mathbf{r}-\mathbf{r}_A|^3}d\Pi \tag{7b}$$

where Π is the Earth volume. Let σ_0 be the averaged mass density of the solid Earth. Then Eq.(7b) becomes

$$\mathbf{F}_N(\mathbf{r}_A) = -m_A\frac{GM}{|\mathbf{r}_A|^3}\mathbf{r}_A + Gm_A\iiint_\Pi \frac{[\sigma(\mathbf{r})-\sigma_0]}{|\mathbf{r}-\mathbf{r}_A|^3}(\mathbf{r}-\mathbf{r}_A)d\Pi \tag{8}$$

Combine the true gravitational force ($\mathbf{F}_N$) and the centrifugal force ($\mathbf{F}_C$) on the point mass A in atmosphere

$$\mathbf{F}(\mathbf{r}_A) = \mathbf{F}_N(\mathbf{r}_A) + \mathbf{F}_C(\mathbf{r}_A) = -m_A g_0\frac{\mathbf{r}_A}{|\mathbf{r}_A|} + m_A\boldsymbol{\Omega}\times(\boldsymbol{\Omega}\times\mathbf{r}_A) + Gm_A\iiint_\Pi \frac{[\sigma(\mathbf{r})-\sigma_0]}{|\mathbf{r}-\mathbf{r}_A|^3}(\mathbf{r}-\mathbf{r}_A)d\Pi \tag{9}$$

Correspondingly the true Earth gravity on the point mass m_A in atmosphere [using Eqs.(2) and (9)] is given by

$$\mathbf{g} = \mathbf{g}_{eff} + \delta\mathbf{g}, \quad \delta\mathbf{g} \equiv \frac{1}{m_A}\left[\mathbf{F}_N(\mathbf{r}_A) - \mathbf{F}_N^{(O)}(\mathbf{r}_A)\right] = G\iiint_\Pi \frac{[\sigma(\mathbf{r})-\sigma_0]}{|\mathbf{r}-\mathbf{r}_A|^3}(\mathbf{r}-\mathbf{r}_A)d\Pi \tag{10}$$

Here, $\mathbf{g}$ is the true gravity; $\delta\mathbf{g}$, with evident horizontal components, is the true gravitational acceleration minus untrue gravitational acceleration, and called the gravity disturbance vector. $\delta\mathbf{g}$ is a major variable and quantified by gravity field models along with observations in geodesy and solid Earth dynamics, however, it is totally neglected in atmospheric dynamics and modeling.

The gravity disturbance vector $\delta\mathbf{g}$ was recently found important in ocean dynamics especially in Ekman transport [7]. However, importance of $\delta\mathbf{g}$ in large-scale atmospheric dynamics has not been recognized. The objective of this study is to show the importance of $\delta\mathbf{g}$ in atmospheric dynamics.

Preprints (www.preprints.org) | NOT PEER-REVIEWED | Posted: 7 February 2023 doi:10.20944/preprints202302.0127.v1

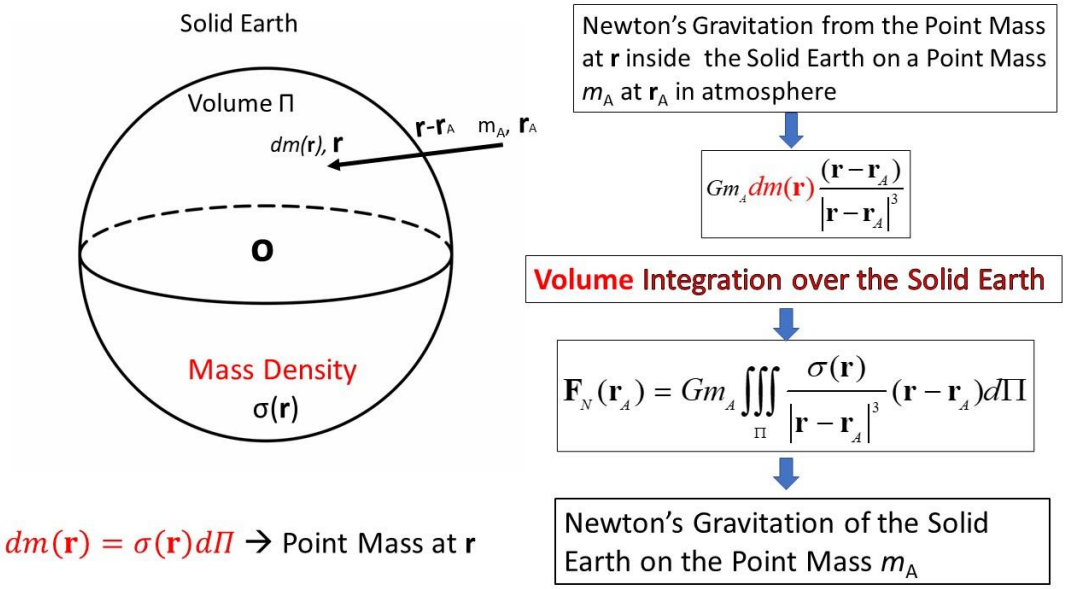

Figure 2. The true Earth gravitation on a point mass m_A at $\mathbf{r}_A$ [i.e., $\mathbf{F}_N(\mathbf{r}_A)$] is the volume integration of Newton's universal gravitation over all point-masses inside the Earth

2. Materials and Methods

2.1. True geopotential

The gravity disturbance vector $\delta\mathbf{g}$ due to the nonuniform mass density $\sigma(\mathbf{r})$ inside the Earth [i.e., $\sigma(\mathbf{r}) \neq \sigma_0$, see Eq.(10)] is represented by the disturbing gravity potential T ($\delta\mathbf{g} \equiv \nabla_3 T$) with ∇_3 the three dimensional vector differential operator. The true geopotential (Φ) is given by [8]

$$\Phi = \Phi_{eff} - T(\lambda, \varphi, z) \tag{11}$$

Due to independence of $\delta\mathbf{g}$ on the Earth rotation [see Eq.(10)], the disturbing gravity potential T outside the Earth masses can be expanded in the polar spherical coordinates [9]

$$T(\lambda,\varphi,z) = \frac{GM}{(R+z)} \sum_{l=2}^{l_{max}} \sum_{m=0}^{l} \left(\frac{R}{R+z}\right)^l \left[\left(C_{l,m} - C_{l,m}^{el}\right)\cos m\lambda + S_{l,m}\sin m\lambda\right] P_{l,m}(\sin\varphi)$$

(12)

where R = 6.3781364×10^6 m is the Earth radius; ($C_{l,m}$, $C_{l,m}^{el}$, $S_{l,m}$) are the harmonic geopotential coefficients with $C_{l,m}^{el}$ belonging to the reference ellipsoid; $P_{l,m}(\sin\varphi)$ are the Legendre associated functions with (l, m) the degree and order of the harmonic expansion; and l_{max} is the order of the gravity field model. The larger the value of l_{max}, the higher the resolution of the disturbing gravity potential T.

Usually, a static gravity field model in geodetic community provides the data for disturbing gravity potential T at z = 0,

Preprints (www.preprints.org) | NOT PEER-REVIEWED | Posted: 7 February 2023 doi:10.20944/preprints202302.0127.v1

$$T(\lambda,\varphi,0)=\frac{GM}{R}\sum_{l=2}^{l_{\max}}\sum_{m=0}^{l}\left[\left(C_{l,m}-C_{l,m}^{el}\right)\cos m\lambda+S_{l,m}\sin m\lambda\right]P_{l,m}(\sin\varphi),$$
$$T_z(\lambda,\varphi,0)=\frac{\partial T(\lambda,\varphi,0)}{\partial z} \quad (13)$$

where T_z (vertical component of the gravity disturbance vector $\delta\mathbf{g}$) is called the gravity disturbance in geodesy. According to (12), the ratio between $T(\lambda, \varphi, z)$ and $T(\lambda, \varphi, 0)$ through the troposphere can be roughly estimated by

$$\left|\frac{T(\lambda,\varphi,z)}{T(\lambda,\varphi,0)}\right|\approx\frac{R}{(R+z)}, \quad H\geq z\geq 0 \quad (14)$$

where H is the height of the troposphere. Because the Earth radius (R) is more than 3 orders of magnitude larger than H, the disturbing gravity potential at the surface (z =0), $T(\lambda, \varphi, 0)$, and its z-derivative $T_z(\lambda, \varphi, 0)$ are used approximately for the whole troposphere in this study,

$$T(\lambda,\varphi,z)\approx T(\lambda,\varphi,0),\ T_z(\lambda,\varphi,z)\approx T_z(\lambda,\varphi,0), \quad H\geq z\geq 0 \quad (15)$$

Besides, the surface disturbing gravity potential $T(\lambda, \varphi, 0)$ is related to the geoid height (N) by the Bruns' formula [10]

$$T(\lambda,\varphi,0)=g_0N(\lambda,\varphi) \quad (16)$$

where N is the geoid undulation. Substitution of (15) into (11) leads to the true geopotential in the troposphere approximately given by

$$\boxed{\Phi=\Phi_{eff}-T\approx\Phi_{eff}-g_0N(\lambda,\varphi)} \quad (17)$$

2.2. Data sources

Two independent and publicly available datasets are used in this study: (a) ICGEM global static gravity field model EIGEN-6C4 (http://icgem.gfz-potsdam.de/home) [9] for [$N(\lambda, \varphi)$, $T_z(\lambda, \varphi, 0)$], and (b) NCEP/NCAR reanalyzed monthly long-term mean (effective) geopotential height (Z), wind velocity (u, v), and temperature (T_a) at 12 pressure levels 1,000, 925, 850, 700, 600, 500, 400, 300, 250, 200, 150, and 100 hPa (https://psl.noaa.gov/data/gridded/data.ncep.reanalysis.derived.pressue.html), are used to identify the importance of the gravity disturbance vector $\delta\mathbf{g}$ on atmospheric dynamics. The long-term annual mean (Z, u, v, T_a) are calculated from the long-term monthly mean data before the identification. The horizontal variability of N shows a range from a minimum of -106.2 m to a maximum of 85.83 m with a mean of 30.57 m (Figure 3a), which is comparable to the horizontal variability of Z at 1,000 hPa (-140 m to 240 m) (Figure 4a). The horizontal variability of T_z shows a range from a minimum of -302.3 mGal to a maximum of 534 mGal with a mean of 39.45 mGal (1 mGal = 10^{-5} m s^{-2}) (Figure 3b).

Preprints (www.preprints.org) | NOT PEER-REVIEWED | Posted: 7 February 2023 doi:10.20944/preprints202302.0127.v1

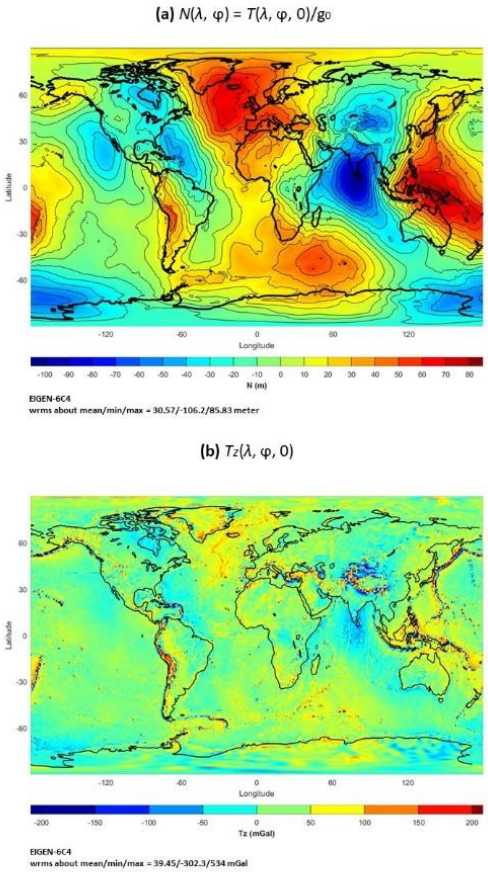

Figure 3. (a) Geoid undulation $N(\lambda, \varphi)$, and (b) gravity disturbance $T_z(\lambda, \varphi, 0)$, obtained online at the website: http://icgem.gfz-potsdam.de/home

Note that the EIGEN-6C4 [$N(\lambda, \varphi)$, $T_z(\lambda, \varphi, 0)$] data are represented in the polar spherical coordinate system since the gravity disturbance vector $\delta\mathbf{g}$ is independent on the Earth rotation [see Eq.(10)]. However, the NCEP/NCAR reanalyzed (Z, u, v, T_a) data are represented in the effective geopotential coordinate system (i.e., the oblate spheroidal coordinates) with the pressure as the vertical coordinate. The difference between the polar spherical and oblate spheroidal coordinate systems are estimated less than 0.17% [2] (P92), and likely to be small except perhaps in long-term simulations in which small systematic differences may accumulate [11-12]. In this study, all the computation is in the polar spherical coordinates including the NCEP/NCAR reanalyzed data. The effect of the gravity disturbance vector ($\delta\mathbf{g}$) on atmospheric dynamics is negligible if the ratio of forcing terms due to the gravity disturbance vector over due to the others (such as the horizontal pressure gradient, and Coriolis force) is comparable to or not substantially larger than the error of using the polar spherical coordinates for the meteorological datasets (i.e., 0.17%) [2] (P92).

Preprints (www.preprints.org) | NOT PEER-REVIEWED | Posted: 7 February 2023 doi:10.20944/preprints202302.0127.v1

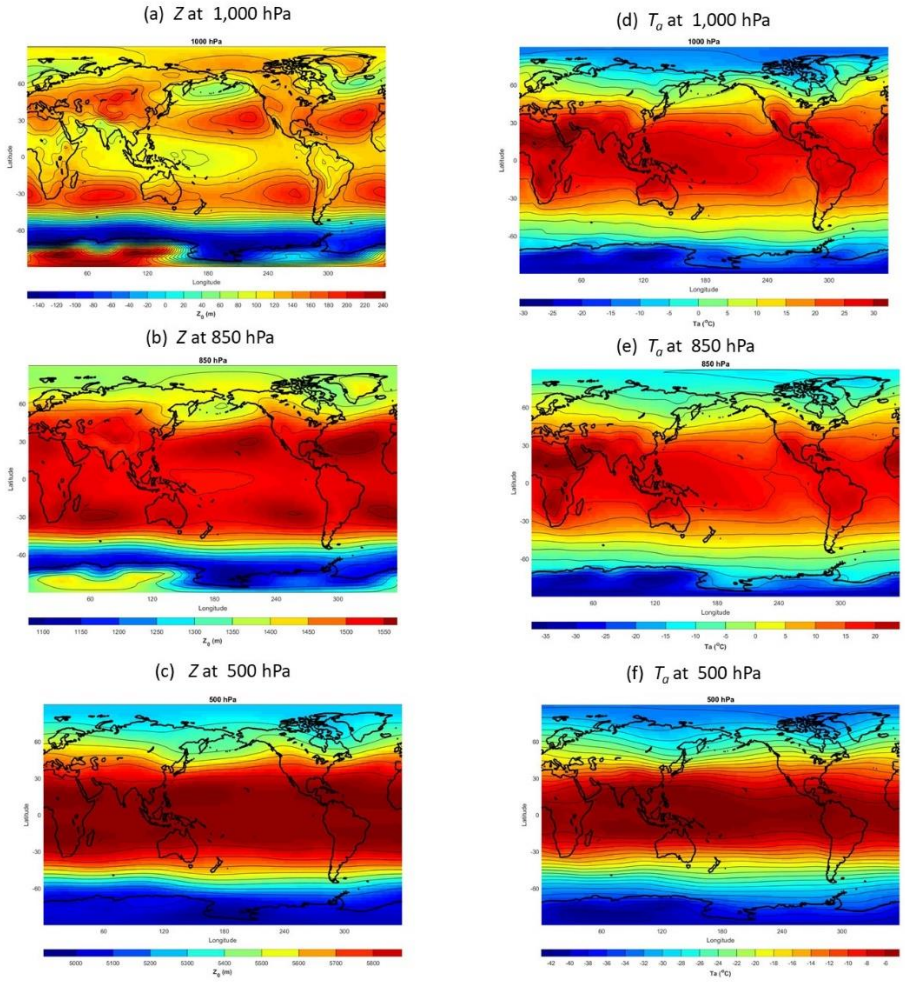

Figure 4. Long-term annual mean data with 2.5°×2.5° resolution on the three pressure levels: geopotential height (Z) at (a) 1,000 hPa, (b) 500 hPa, and (c) 100 hPa, and temperature (T_a) at (d) 1,000 hPa, (e) 500 hPa, and (f) 100 hPa. The data were calculated from the long-term monthly mean Z and T_a obtained online at the website: https://psl.noaa.gov/data/gridded/data.ncep.reanalysis.derived.html

2.3. Horizontal gradients of T in pressure as vertical coordinate

Consider the local effective geopotential coordinate system with z as the vertical coordinate (i.e., the direction of **k**) and (x, y) the horizontal coordinates. A derivative with respect to x between the z and p as the vertical coordinates is given by

$$\left(\frac{\partial}{\partial x}\right)_p = \left(\frac{\partial}{\partial x}\right)_z + \left(\frac{\partial z}{\partial x}\right)_p \frac{\partial}{\partial z} \tag{18}$$

Using (18) to the derivative of p gives

$$0 = \left(\frac{\partial p}{\partial x}\right)_z + \left(\frac{\partial z}{\partial x}\right)_p \frac{\partial p}{\partial z},$$

(19)

and to the derivative of T gives

$$\left(\frac{\partial T}{\partial x}\right)_p = \left(\frac{\partial T}{\partial x}\right)_z + \left(\frac{\partial z}{\partial x}\right)_p \frac{\partial T}{\partial z}$$

(20)

Here, the hydrostatic balance is represented by

Preprints (www.preprints.org) | NOT PEER-REVIEWED | Posted: 7 February 2023 doi:10.20944/preprints202302.0127.v1

$$\frac{\partial p}{\partial z} = -\rho g_0, \quad \Phi_{eff} = g_0 z$$

(21)

Elimination of $(\partial z / \partial x)_p$ from (19) and (20) and use of (21) give

$$\left(\frac{\partial T}{\partial x}\right)_z = \left(\frac{\partial T}{\partial x}\right)_p - \left(\frac{\partial \Phi_{eff}}{\partial x}\right)_p \left(\frac{1}{g_0}\frac{\partial T}{\partial z}\right)$$

(22)

With the same procedure for the derivative of T with respect to y, we have

$$\nabla_z T = \nabla T - (T_z / g_0)\nabla \Phi_{eff}$$

(23)

where ∇ (or ∇_z) is the horizontal vector differential operator in p (or z) as the vertical coordinate. Figure 3b shows that T_z varies between -302.3 mGal and 534.0 mGal, which leads to

$$\boxed{|T_z / g_0| < 534 \text{ mGal}/(9.81 \text{ m s}^{-2}) = 5.443\times10^{-4}} \quad (24)$$

3. Results

3.1. Equation of motion with the true geopotential

With the true geopotential (Φ), the horizontal component of the dynamic equation in the pressure as the vertical coordinate is given by

$$\frac{D\mathbf{U}}{Dt} + f\mathbf{k}\times\mathbf{U} = -\nabla\Phi + \mathbf{F} \quad (25)$$

where f is the Coriolis parameter; $\mathbf{U} = (u, v)$, is the horizontal velocity vector; $\mathbf{F}$ is the frictional force; and

$$\frac{D}{Dt} = \frac{\partial}{\partial t} + \mathbf{U}\bullet\nabla + \omega\frac{\partial}{\partial p}, \quad \omega = \frac{dp}{dt} \quad (26)$$

Here, ω is the vertical velocity in the pressure as the vertical coordinate. Substitution of (11) into (25) leads to

$$\boxed{\frac{D\mathbf{U}}{Dt} + f\mathbf{k}\times\mathbf{U} = -\nabla\Phi_{eff} + \nabla T + \mathbf{F}, \quad \Phi_{eff} = g_0 Z}$$

(27)

Substitution of (23) into (27) lead to

$$\frac{D\mathbf{U}}{Dt} + f\mathbf{k}\times\mathbf{U} = -\left[1-(T_z / g_0)\right]\nabla\Phi_{eff} + \nabla_z T + \mathbf{F}$$

which gives

$$\frac{D\mathbf{U}}{Dt} + f\mathbf{k}\times\mathbf{U} = -\nabla\Phi_{eff} + \nabla_z T + \mathbf{F} \quad (28)$$

Here, the inequality (24) is used. Eq.(28) shows that the horizontal gradient ∇T (or ∇N) in p as the vertical coordinate can be replaced by $\nabla_z T$ (or $\nabla_z N$) in z as the vertical coordinate,

$$\boxed{T = g_0 N, \quad \nabla T \equiv \text{horizontal component of } \delta\mathbf{g} \approx \nabla_z T, \quad \nabla^2 T \approx \nabla_z^2 T}$$

(29)

Preprints (www.preprints.org) | NOT PEER-REVIEWED | Posted: 7 February 2023 doi:10.20944/preprints202302.0127.v1

Non-dimensional B and C numbers are defined by

$$B \equiv \frac{O(|\nabla T|)}{O(|\nabla \Phi_{eff}|)} \approx \frac{g_0 O(|\nabla_z N|)}{O(|\nabla \Phi_{eff}|)} = \frac{O(|\nabla_z N|)}{O[|\nabla Z|]}, \quad C \equiv \frac{O(|\nabla T|)}{O(|f\mathbf{U}|)} \approx \frac{g_0 O(|\nabla_z N|)}{O(|f\mathbf{U}|)} \tag{30}$$

to identify the importance of the gravity disturbance vector ($\delta\mathbf{g}$) versus the effective gravity ($\mathbf{g}_{eff}$) (B number) and the Coriolis force (C number). Here (15), (16), and (29) are used. Hereafter the global mean is taken to represent the order of magnitude. Eq. (30) becomes

$$B = \frac{\text{mean}(|\nabla_z N|)}{\text{mean}[|\nabla Z|]}, \quad C = g_0 \frac{\text{mean}(|\nabla_z N|)}{\text{mean}(|f\mathbf{U}|)} \tag{31}$$

The global long-term annual mean geopotential height Z has comparable horizontal variability at 1,000 hPa (Figure 4a) as the geoid N (Figure 3a), becomes near zonal at 850 hPa (Figure 4b) and 500 hPa (Figure 4c). The vector $\nabla_z N$ (Figure 5a) is $\nabla_z T/g_0$ at $z = 0$. The histogram of $|\nabla_z N|$ (Figure 5b) shows a positively skewed distribution with a long tail and mean of 2.360×10^{-5}. The two vector fields $\nabla_z N$ (Figure 5a) and ∇Z (Figures 6a-c) are quite different. The difference becomes larger as p-level decreasing from 1,000 hPa (Figure 6a) to 500 hPa (Figure 6c). The vector ∇Z is near latitudinal at 500 hPa (Figure 6c). The histograms of $|\nabla Z|$ show positively skewed distributions with mean of 5.824×10^{-5} at 1,000 hPa (Figure 6d), 5.651×10^{-5} at 850 hPa (Figure 6e), and 8.285×10^{-5} at 500 hPa (Figure 6f).

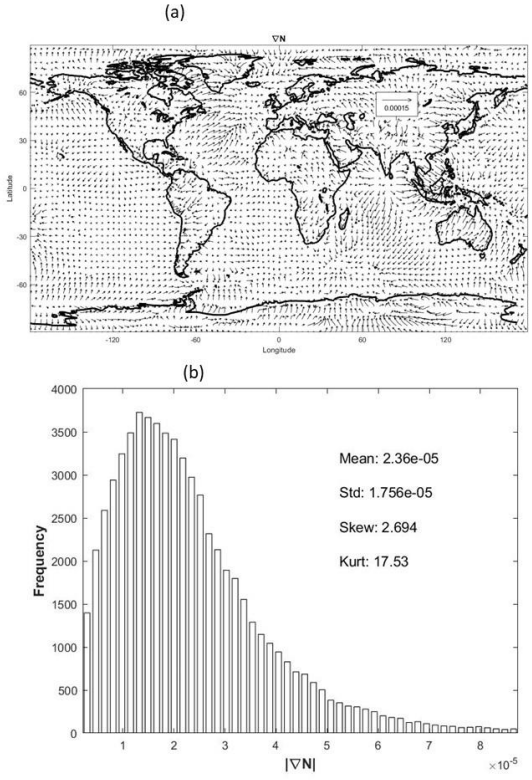

Figure 5. (a) Vector plot of $\nabla_z N$ and (b) histogram of $|\nabla_z N|$ with four statistical parameters (mean, standard deviation, skewness, kurtosis).

Preprints (www.preprints.org) | NOT PEER-REVIEWED | Posted: 7 February 2023 doi:10.20944/preprints202302.0127.v1

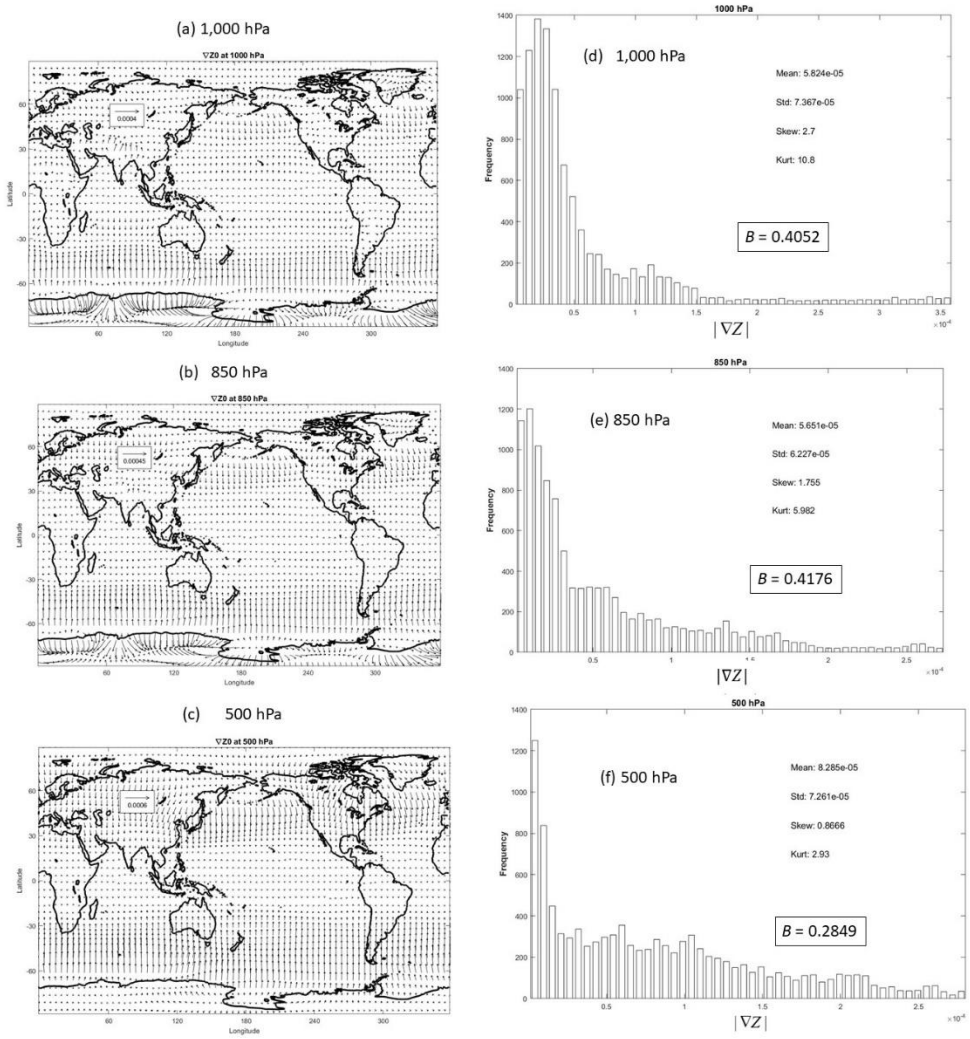

Figure 6. Vector plot of ∇*Z* on (a) 1,000 hPa, (b) 850 hPa, and (c) 500 hPa, and histograms of $|\nabla Z|$ with four statistical parameters (mean, standard deviation, skewness, kurtosis) and *B* number on (d) 1,000 hPa, (e) 850 hPa, and (f) 500 hPa.

The global long-term annual mean wind vectors (**U**) show the general circulation at 1,000 hPa (Figure 7a), 500 hPa (Figure 7b), and 100 hPa (Figure 7c). The magnitude of the Coriolis force is represented by $|f\mathbf{U}|$. The histogram of $|f\mathbf{U}|$ shows a positively skewed distribution with mean of 37.53 mGal at 1,000 hPa (Figure 7d), 49.01 mGal at 850 hPa (Figure 7e), and 83.19 mGal at 500 hPa (Figure 7f). The global mean of the horizontal gradient of disturbing geopotential ($\nabla_z T = g_0 \nabla_z N$) is 23.15 mGal.

Preprints (www.preprints.org) | NOT PEER-REVIEWED | Posted: 7 February 2023 doi:10.20944/preprints202302.0127.v1

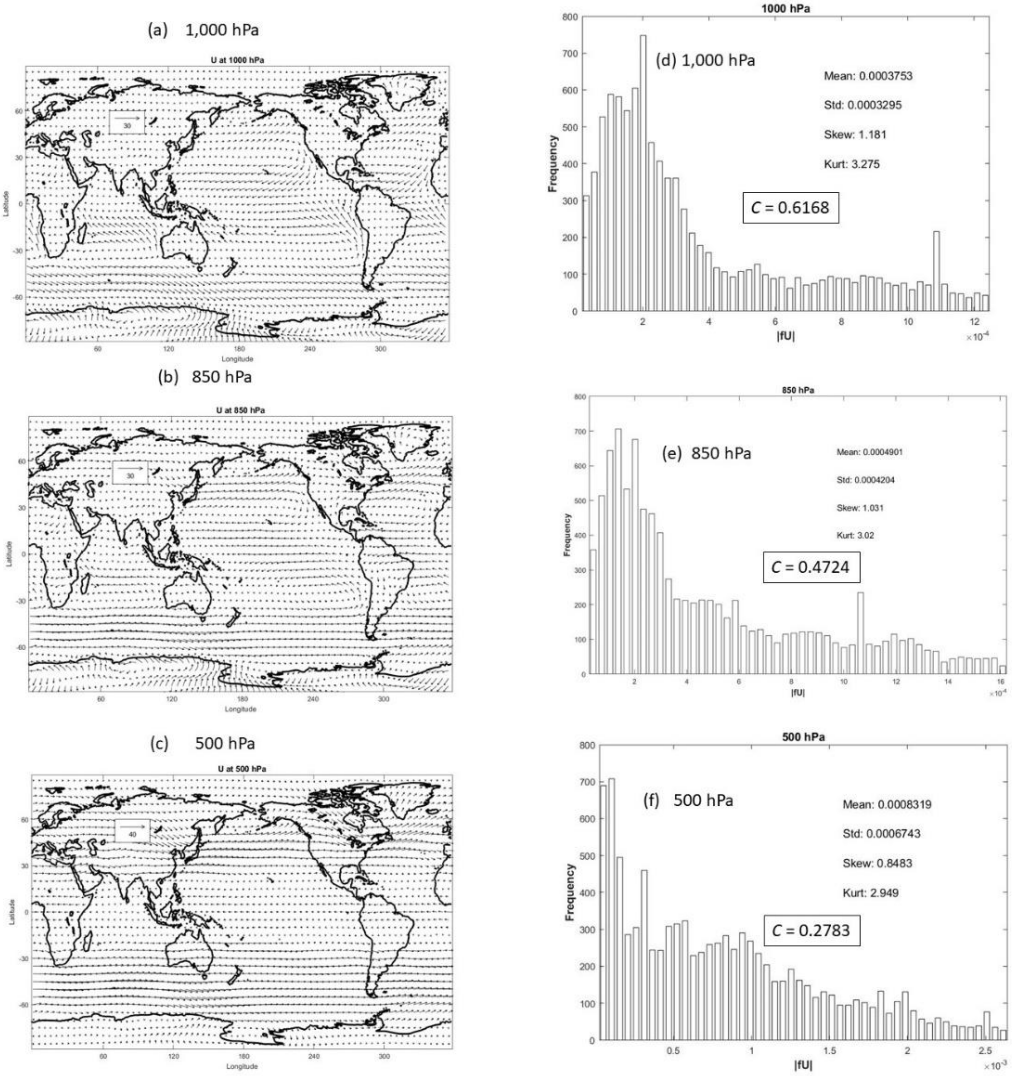

Figure 7. Vector plots of long-term annual mean wind vectors (U) on (a) 1,000 hPa, (b) 850 hPa, and (c) 500 hPa, and histograms of |U| with four statistical parameters (mean, standard deviation, skewness, kurtosis) and *C* number on (d) 1,000 hPa, (e) 850 hPa, and (f) 500 hPa. The long-term annual mean wind vector U were calculated from the long-term monthly mean wind vector U obtained online at the website: https://psl.noaa.gov/data/gridded/data.ncep.reanalysis.derived.html.

Both *B* and *C* numbers are not small. The *B*-number has a maximum of 0.4176 at 850 hPa and a minimum of 0.1630 at 200 hPa. It is greater than 0.28 for 1,000-500 hPa (Table 1). The *C*-number has a maximum of 0.6168 at 1,000 hPa, a minimum of 0.1573 at 200 hPa. It is greater than 0.27 for 1,000-500 hPa (Table 2).

Preprints (www.preprints.org) | NOT PEER-REVIEWED | Posted: 7 February 2023 doi:10.20944/preprints202302.0127.v1

Table 1. Global means of $|\nabla_z N|$ and annual $|\nabla Z|$ at 12 pressure levels in the troposphere (treated as the order of magnitude) as well as the non-dimensional B-number.

Pressure Level (hPa)	Mean ($\|\nabla Z\|$) (10^{-5})	Mean ($\|\nabla_z \boldsymbol{N}\|$) ($10^{-5}$)	B-number
		2.360	
1,000	5.824		0.4052
925	5.686		0.4151
850	5.651		0.4176
700	6.153		0.3836
600	6.870		0.3435
500	8.285		0.2849
400	10.27		0.2298
300	12.68		0.1861
250	13.78		0.1713
200	14.48		0.1630
150	14.40		0.1639
100	12.63		0.1869

Preprints (www.preprints.org) | NOT PEER-REVIEWED | Posted: 7 February 2023 doi:10.20944/preprints202302.0127.v1

Table 2. Global means of ($g_0|\nabla N|$) and annual $|f\mathbf{U}|$ at 12 pressure levels in the troposphere (treated as the order of magnitude) as well as the non-dimensional *C*-number.

Pressure Level (hPa)	Mean ($|f\mathbf{U}|$) (mGal)	Mean ($g_0|\nabla N|$) (mGal)	*C*-number
		23.15	
1,000	37.53		0.6168
925	45.52		0.5086
850	49.01		0.4724
700	60.46		0.3829
600	69.59		0.3327
500	83.19		0.2783
400	103.3		0.2241
300	128.8		0.1797
250	140.7		0.1645
200	147.2		0.1573
150	143.7		0.1611
100	126.0		0.1837

3.2. Hydrostatic equilibrium

The hydrostatic equilibrium [represented by the superscript (HE)] is defined by the coincidence of the geopotential surface with the isobaric surface. For the effective geopotential Φ_{eff}, we have

$$\boxed{\Phi_{eff}^{(HE)}(\text{or } Z^{(HE)}) = \text{const at isobaric surface} \Leftrightarrow \nabla\Phi_{eff}^{(HE)} = 0 \Leftrightarrow \nabla Z^{(HE)} = 0} \tag{32a}$$

For the true geopotential Φ, we get

$$\boxed{\begin{aligned}&\Phi^{(HE)}[\text{or } (Z^{(HE)} - N)] = \text{const at isobaric surface}\\ &\Leftrightarrow \nabla\Phi^{(HE)} = 0 \Leftrightarrow \nabla(Z^{(HE)} - N) = 0 \Leftrightarrow \nabla Z^{(HE)} = \nabla N\end{aligned}} \tag{32b}$$

Here, $\Phi_{eff}^{(HE)}$ and $\Phi^{(HE)}$ are the hydrostatic equilibria of the effective and true geopotentials; $Z^{(HE)}$ is the hydrostatic equilibrium of the geopotential height. Obviously, the hydrostatic equilibrium is different between the effective geopotential (Φ_{eff}) and the true geopotential (Φ).

3.3. Geostrophic wind

Steady state flow without friction leads to the geostrophic balance from Eq.(27)

$$\boxed{f\mathbf{k}\times\mathbf{U}_g = -\nabla\Phi_{eff} + \nabla T} \tag{33}$$

which is rewritten by

$$\boxed{\mathbf{U}_g = \frac{\mathbf{k}}{f}\times\left[\nabla\Phi_{eff} - \nabla T\right]} \tag{34}$$

The geostrophic wind is decomposed into two parts, $\mathbf{U}_g = \mathbf{U}_{g0} + \mathbf{U}_{g\delta}$, with

$$\mathbf{U}_{g0} = \frac{\mathbf{k}}{f}\times\nabla\Phi_{eff} = \frac{g_0}{f}\mathbf{k}\times\nabla Z \tag{35}$$

Preprints (www.preprints.org) | NOT PEER-REVIEWED | Posted: 7 February 2023 doi:10.20944/preprints202302.0127.v1

which represents the classical geostrophic wind, and

$$\mathbf{U}_{g\delta} = -\frac{\mathbf{k}}{f}\times\nabla T \approx -\frac{g_0\mathbf{k}}{f}\times\nabla N \tag{36}$$

which denotes the geostrophic wind due to the gravity disturbance vector $\delta\mathbf{g}$. Obviously, the non-dimensional B number (31) is also the ratio between $O(|\mathbf{U}_{g\delta}|)$ and $O(|\mathbf{U}_{g0}|)$,

$$\frac{O(|\mathbf{U}_{g\delta}|)}{O\left[|\mathbf{U}_{g0}|\right]} = \frac{g_0 O(|\nabla_z N|)}{O(|\nabla\Phi_{eff}|)} = \frac{O(|\nabla_z N|)}{O(|\nabla Z|)} = \frac{\text{mean}(|\nabla_z N|)}{\text{mean}(|\nabla Z|)}$$
$$= B = \begin{cases} 0.4176 \text{ (max) at 850 hPa} \\ 0.1630 \text{ (min) at 200 hPa} \end{cases} \tag{37}$$

The B number listed in Table 1 from 1,000 hPa to 100 hPa demonstrates that the gravity disturbance vector ($\delta\mathbf{g}$) is nonnegligible in the geostrophic wind.

3.4. Thermal wind

Differentiation of the geostrophic wind equation (34) with respect to p leads to

$$\frac{\partial\mathbf{U}_g}{\partial p} = \frac{\mathbf{k}}{f}\times\left[\nabla\left(\frac{\partial\Phi_{eff}}{\partial p}\right) - \nabla\left(\frac{\partial T}{\partial p}\right)\right] \tag{38}$$

Since

$$\frac{\partial T}{\partial p} = \frac{\partial T/\partial z}{\partial p/\partial z} = -\frac{\partial T/\partial z}{\rho g_0}, \quad \frac{\partial\Phi_{eff}}{\partial p} = -\frac{1}{\rho}, \quad \rho = \frac{p}{R_a T_a} \tag{39}$$

substitution of (39) into (38) leads to

$$\frac{\partial\mathbf{U}_g}{\partial p} = \frac{\mathbf{k}}{f}\times\left[\nabla\left(-\frac{R_a T_a}{p}\right)\right]\left(1-\frac{T_z}{g_0}\right) + \frac{R_a T_a}{p}\frac{\mathbf{k}}{f}\times\nabla\left(\frac{T_z}{g_0}\right) \tag{40}$$

where R_a = 287 JK^{-1}kg^{-1}, is the gas constant for dry air. Since $|T_z|/g_0 < 5.443\times10^{-4}$ [see Eq.(24)] and should be neglected against 1. Eq.(40) becomes

$$\frac{\partial\mathbf{U}_g}{\partial\ln p} == -\frac{R_a\mathbf{k}}{f}\times\nabla T_a + \frac{R_a T_a}{g_0}\frac{\mathbf{k}}{f}\times\nabla T_z \tag{41}$$

The nondimensional A number is defined by

$$A = \frac{O\left[|\nabla T_z|/g_0\right]}{O\left[|\nabla T_a|/T_a\right]} \approx \frac{O\left[|\nabla_z T_z|/g_0\right]}{O\left[|\nabla T_a|/T_a\right]} \tag{42}$$

to identify relative importance of the gravity disturbance vector ($\delta\mathbf{g}$) versus the effective gravity ($\mathbf{g}_{eff}$) on the thermal wind relation.

The variable $|\nabla_z T_z|/g_0$ is calculated from the static gravity field model EIGEN-6C4 T_z data (Figure 8a). The variable $|\nabla T_a|/T_a$ is computed from the NCEP/NCAR reanalyzed global long-term annual mean air temperature T_a at 12 pressure levels such as at 1,000 hPa (Figure 8b), 850 hPa (Figure 8c), and 500 hPa (Figure 8d). The histogram of $|\nabla_z T_z|/g_0$ shows a positively skewed distribution with the mean of 1.144×10^{-10}m^{-1} (Figure 9a). The histograms of $|\nabla T_a|/T_a$ also show positively skewed distributions with the mean of 2.192×10^{-8}m^{-1} at 1,000 hPa (Figure 9b), with the mean of

Preprints (www.preprints.org) | NOT PEER-REVIEWED | Posted: 7 February 2023 doi:10.20944/preprints202302.0127.v1

1.954×10^{-8}m^{-1} at 850 hPa (Figure 9c), and a bi-modal distribution with the mean of 1.402×10^{-8}m^{-1} at 500 hPa (Figure 9d). The A number varies from 0.5219×10^{-2} (min) at 1,000 hPa to 1.9816×10^{-2} (max) at 200 hPa (Table 3). Such small values of the A number demonstrate the second term in the righthand side of (41) negligible,

$$\frac{\partial \mathbf{U}_g}{\partial \ln p} = -\frac{R_d \mathbf{k}}{f} \times \nabla T_a \tag{43}$$

which leads to

$$\frac{\partial \Phi}{\partial p} = \frac{\partial \Phi_{eff}}{\partial p} = -\frac{R_a T_a}{p} \tag{44}$$

which indicates that the thermal wind relation is kept unchanged from using the effective geopotential Φ_{eff} to the true geopotential Φ. This is caused by that the disturbing gravity potential at the surface (z =0), $T(\lambda, \varphi, 0)$, and its z-derivative $T_z(\lambda, \varphi, 0)$ are used approximately for the whole troposphere, see Equation (15).

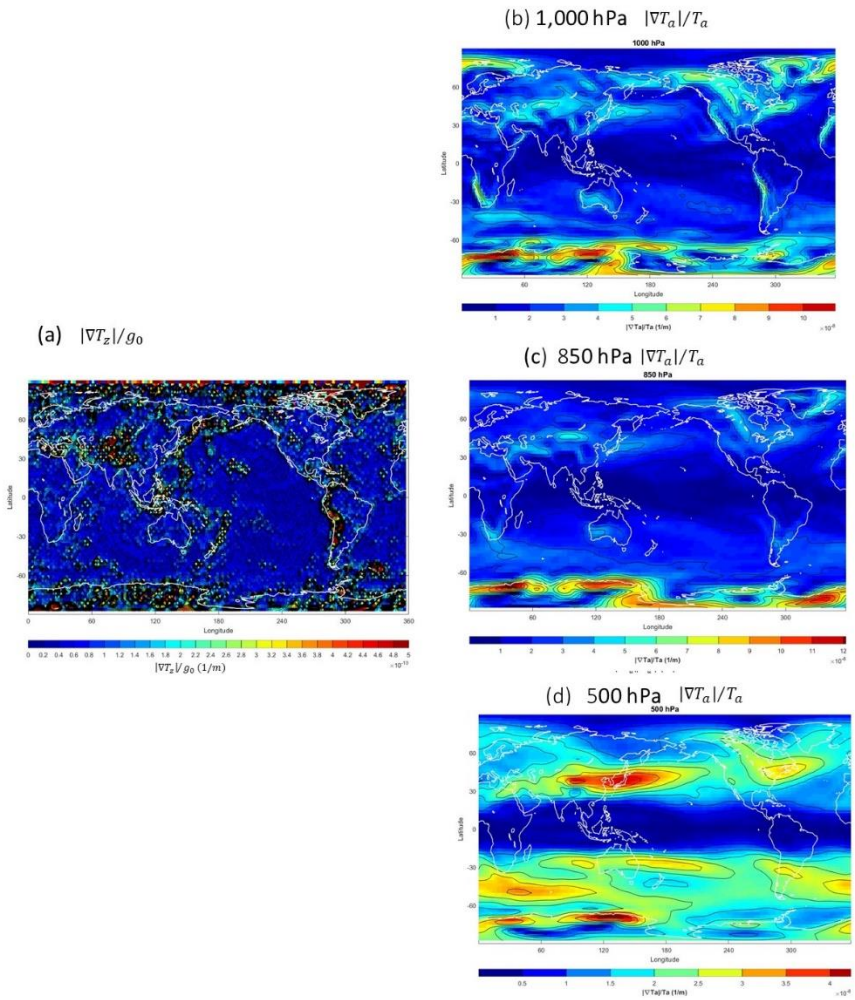

Preprints (www.preprints.org) | NOT PEER-REVIEWED | Posted: 7 February 2023 doi:10.20944/preprints202302.0127.v1

Figure 8. Horizontal distributions of (a) $|\nabla_z T_a|/g_0$, and $|\nabla T_a|/T_a$ on (b) 1,000 hPa, (c) 850 hPa, and (d) 500 hPa.

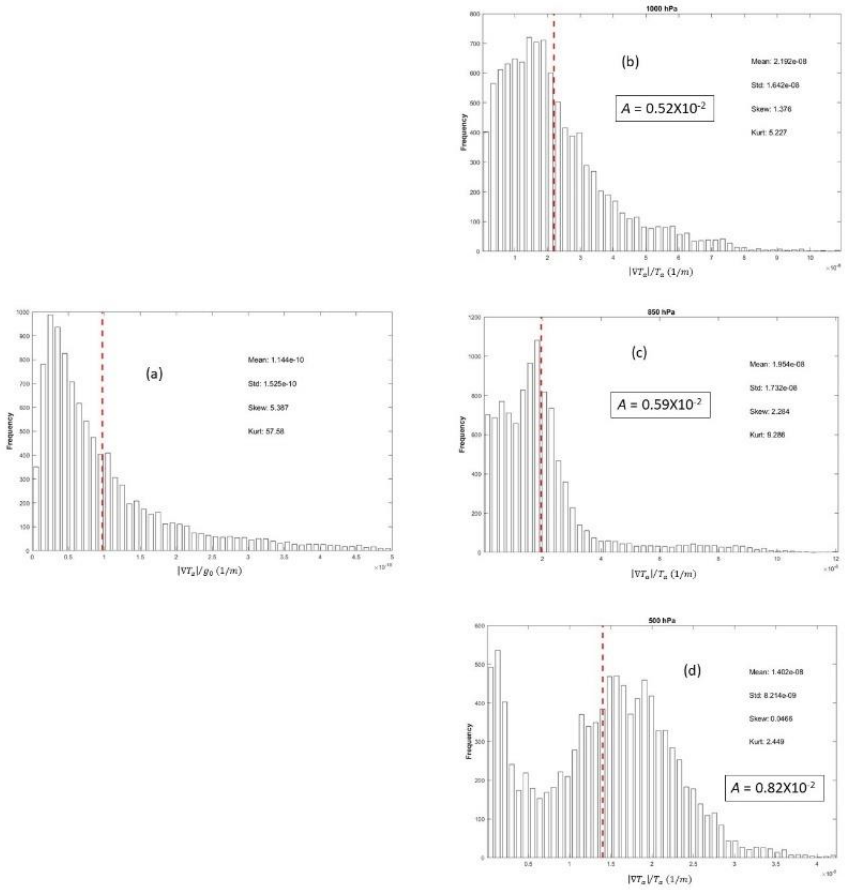

Figure 9. Histograms of (a) $|\nabla_z T_a|/g_0$, and $|\nabla T_a|/T_a$ with four statistical parameters (mean, standard deviation, skewness, kurtosis) and A number on (b) 1,000 hPa, (c) 850 hPa, and (d) 500 hPa. The red dashed lines show the mean values from the corresponding histograms.

Preprints (www.preprints.org) | NOT PEER-REVIEWED | Posted: 7 February 2023 doi:10.20944/preprints202302.0127.v1

Table 3. Global means of $|\nabla_z T_z|/g_0$ and annual $|\nabla T_a|/T_a$ at 12 pressure levels in the troposphere (treated as the order of magnitude) as well as the non-dimensional A-number.

Pressure Level (hPa)	Mean ($\|\nabla T_a\|/T_a$) (10^{-8} m^{-1})	Mean ($\|\nabla_z T_z\|/g_0$) (10^{-8} m^{-1})	A-number
		1.144×10^{-2}	
1,000	2.192		0.5219×10^{-2}
925	2.025		0.5649×10^{-2}
850	1.954		0.5855×10^{-2}
700	1.885		0.6069×10^{-2}
600	1.561		0.7329×10^{-2}
500	1.402		0.8160×10^{-2}
400	1.382		0.8278×10^{-2}
300	1.168		0.9795×10^{-2}
250	0.8997		1.2715×10^{-2}
200	0.5773		1.9816×10^{-2}
150	0.9135		1.2523×10^{-2}
100	1.5140		0.7556×10^{-2}

3.5. Geostrophic vorticity

In p as the vertical coordinate and the Coriolis parameter taken as a constant, the geostrophic relative vorticity is given by

$$\zeta_{eff} = \frac{1}{f}\nabla^2\Phi_{eff} \tag{45a}$$

with the effective gravity ($\mathbf{g}_{eff}$) and is represented by

$$\boxed{\zeta = \frac{1}{f}\nabla^2\Phi = \zeta_{eff} + \zeta_{gd},\quad \zeta_{eff} = \frac{1}{f}\nabla^2\Phi_{eff} = \frac{g_0}{f}\nabla^2 Z,\quad \zeta_{gd} = -\frac{g_0}{f}\nabla^2 N} \tag{45b}$$

with the true gravity ($\mathbf{g}$). Here, Eq.(17) is used and ζ_{gd} represents the geostrophic vorticity due to the gravity disturbance vector ($\delta\mathbf{g}$).

3.6. Ekman pumping

The Ekman pumping velocity at the top of the Ekman layer is given by [1] (P132, Equation 5.38)

$$w(D_E) = \frac{\zeta}{2\gamma} = \frac{1}{2\gamma}(\zeta_{eff} + \zeta_{gd}),\quad \gamma \equiv \left|\frac{f}{2K}\right|^{1/2}\left(\frac{f}{|f|}\right) \tag{46}$$

A nondimensional D number is defined by

$$D \equiv \frac{O(|\zeta_{gd}|)}{O(|\zeta_{eff}|)} = \frac{O[|\nabla^2 N|]}{O[|\nabla^2 Z|]} \approx \frac{O[|\nabla_z^2 N|]}{O[|\nabla^2 Z|]} \tag{47}$$

to identify relative importance of $\delta\mathbf{g}$ versus the effective gravity ($\mathbf{g}_{eff}$) on the geostrophic vorticity and in turn on the Ekman layer dynamics.

Preprints (www.preprints.org) | NOT PEER-REVIEWED | Posted: 7 February 2023 doi:10.20944/preprints202302.0127.v1

The static gravity field model EIGEN-6C4 N data are used to calculate $|\nabla_z^2 N|$ (Figure 10a). The NCEP/NCAR reanalyzed global long-term annual mean geopotential height Z data are used to compute $|\nabla^2 Z|$ for 12 pressure levels such as 1,000 hPa (Figure 10b), 850 hPa (Figure 10c), and 500 hPa (Figure 10d). The histogram of $|\nabla_z^2 N|$ shows a positively skewed distribution with the mean of 0.7833×10^{-10}m^{-1} (Figure 11a). The histograms of $|\nabla^2 Z|$ also show positively skewed distributions with the mean of 1.167×10^{-10}m^{-1} at 1,000 hPa (Figure 11b), with the mean of 0.9179×10^{-10}m^{-1} at 850 hPa (Figure 11c), and with the mean of 0.5854×10^{-10}m^{-1} at 500 hPa (Figure 11d). The D number varies from 0.6712 (min) at 1,000 hPa to 1.3381 (max) at 500 hPa (Table 4). Such values of the D number demonstrate the gravity disturbance vector ($\delta\mathbf{g}$) is non-negligible in comparison to the effective gravity ($\mathbf{g}_{eff}$) on the geostrophic vorticity. Besides, if 850 hPa is treated as the top of the Ekman layer, the Ekman pumping velocity (proportional to the geostrophic vorticity) is comparable due to the effective geopotential $\nabla^2 Z$ and due to the gravity disturbance vector $\nabla_z^2 N$ because B = 0.8534 at 850 hPa.

Preprints (www.preprints.org) | NOT PEER-REVIEWED | Posted: 7 February 2023 doi:10.20944/preprints202302.0127.v1

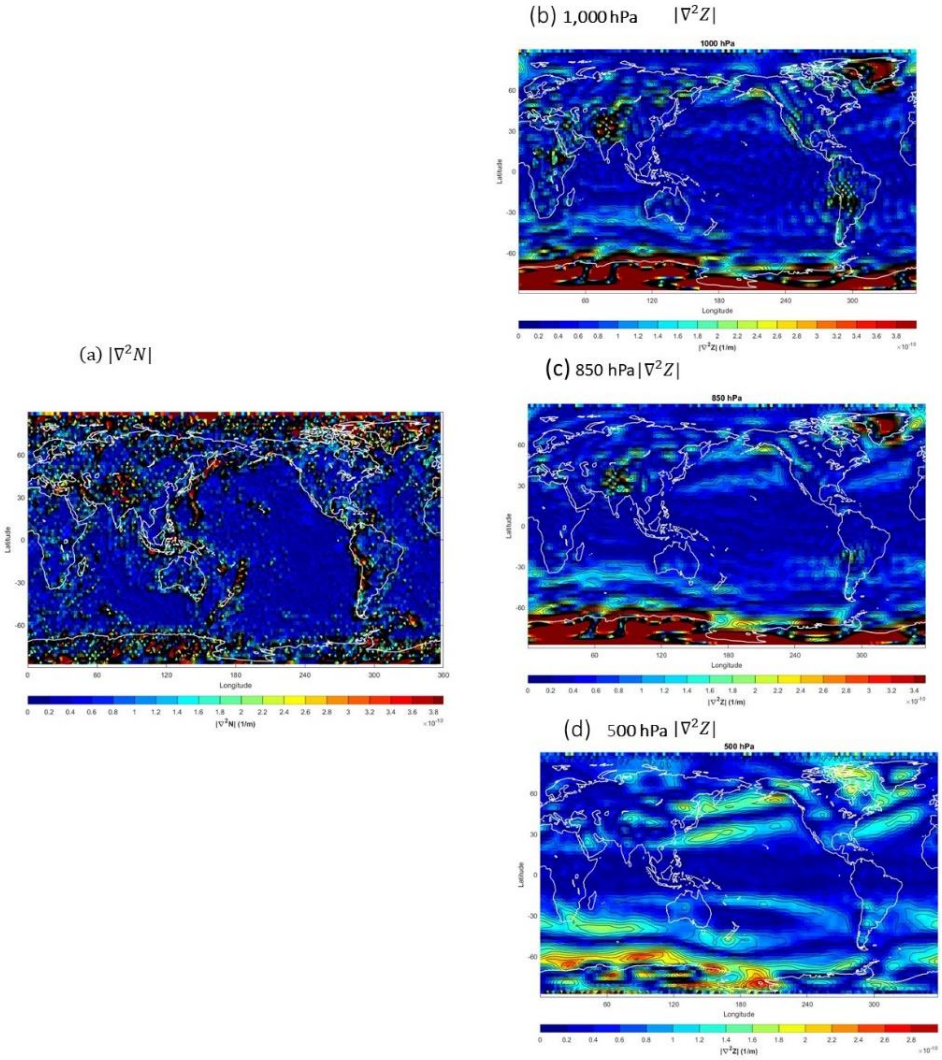

Figure 10. Horizontal distributions of (a) $|\nabla_z^2 N|$ and $|\nabla^2 Z|$ on (b) 1,000 hPa, (c) 850 hPa, and (d) 500 hPa.

Preprints (www.preprints.org) | NOT PEER-REVIEWED | Posted: 7 February 2023 doi:10.20944/preprints202302.0127.v1

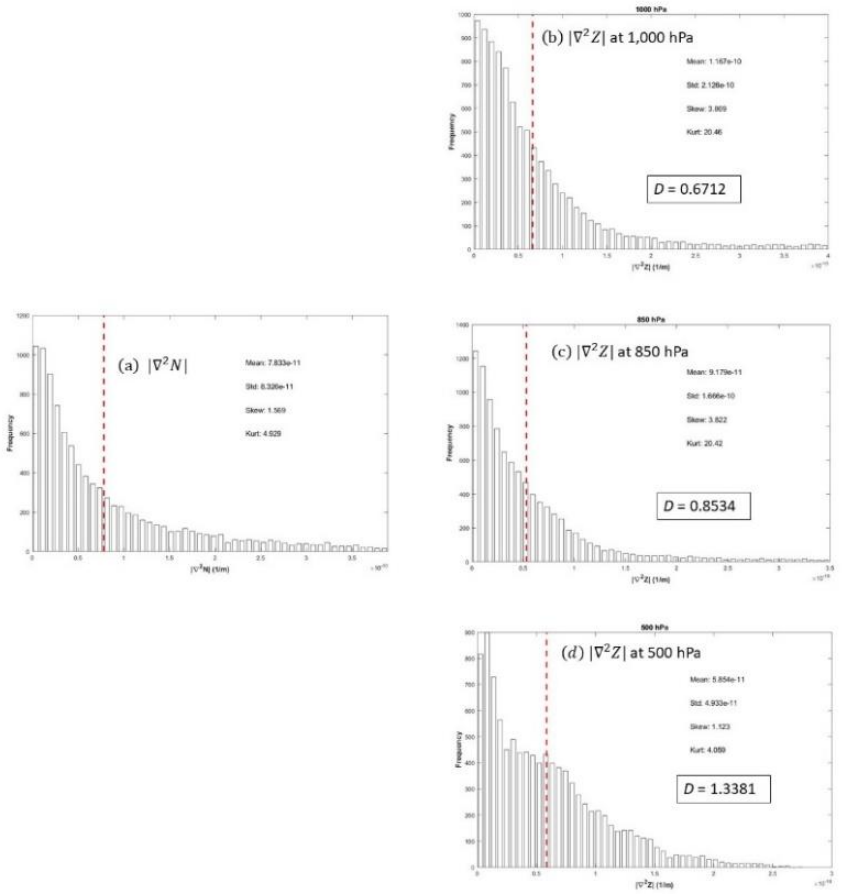

Figure 11. Histograms of (a) $|\nabla_z^2 N|$, and $|\nabla^2 Z|$ with four statistical parameters (mean, standard deviation, skewness, kurtosis) and D number on (b) 1,000 hPa, (c) 850 hPa, and (d) 500 hPa. The red dashed lines show the mean values from the corresponding histograms.

Table 4. Global means of $|\nabla_z^2 N|$ and annual $|\nabla^2 Z|$ at 12 pressure levels in the troposphere (treated as the order of magnitude) as well as the non-dimensional D-number.

Pressure Level (hPa)	Mean ($\|\nabla^2 Z\|$) (10^{-10} m^{-1})	Mean ($\|\nabla_z^2 N\|$) (10^{-10} m^{-1})	D-number
		0.7833	
1,000	1.167		0.6712
925	1.039		0.7539
850	0.9179		0.8534
700	0.7071		1.1078
600	0.5870		1.3344
500	0.5854		1.3381
400	0.6252		1.2529
300	0.7013		1.1169
250	0.7320		1.0701
200	0.7415		1.0564
150	0.7150		1.0955
100	0.6469		1.2109

3.7. Q vector

Preprints (www.preprints.org) | NOT PEER-REVIEWED | Posted: 7 February 2023 doi:10.20944/preprints202302.0127.v1

The Q vector defined by [1] (P170, Equation 6.54)

$$\mathbf{Q} \equiv (Q_1, Q_2) = (-\frac{R_a}{p}\frac{\partial \mathbf{U}_g}{\partial x} \bullet \nabla T_a, \quad -\frac{R_a}{p}\frac{\partial \mathbf{U}_g}{\partial y} \bullet \nabla T_a) \tag{48}$$

is used in atmospheric dynamics to identify physical processes such as vertical motion and frontogenesis on the base of the quasi-geostrophic system. Here, (x, y) are local horizontal coordinates. Substitution of (34) into (48) leads to

$$\mathbf{Q} = \mathbf{Q}^{eff} + \mathbf{Q}^{gd}, \quad \mathbf{Q}^{eff} = (Q_1^{eff}, Q_2^{eff}), \ \mathbf{Q}^{gd} = (Q_1^{gd}, \ Q_2^{gd}) \tag{49}$$

where $\mathbf{Q}^{\text{eff}}$ and $\mathbf{Q}^{\text{gd}}$ are the Q vector associated with the effective gravity and gravity disturbance vector, respectively. Their components are given by

$$\begin{aligned} Q_1^{eff} &= -\frac{R_a}{p}\frac{\partial \mathbf{U}_{g0}}{\partial x} \bullet \nabla T_a = -\frac{R_a g_0}{pf} q_1^{eff}, \quad Q_2^{eff} = -\frac{R_a}{p}\frac{\partial \mathbf{U}_{g0}}{\partial y} \bullet \nabla T_a = -\frac{R_a g_0}{pf} q_2^{eff} \\ Q_1^{gd} &= -\frac{R_a}{p}\frac{\partial \mathbf{U}_{g\delta}}{\partial x} \bullet \nabla T_a = \frac{R_a g_0}{pf} q_1^{gd}, \quad Q_2^{gd} = -\frac{R_a}{p}\frac{\partial \mathbf{U}_{g\delta}}{\partial y} \bullet \nabla T_a = \frac{R_a g_0}{pf} q_2^{gd} \end{aligned} \tag{50}$$

where

$$q_1^{eff} = -J(\frac{\partial Z}{\partial x}, T_a), \quad q_2^{eff} = -J(\frac{\partial Z}{\partial y}, T_a), \ q_1^{gd} = J(\frac{\partial N}{\partial x}, T_a), \quad q_2^{gd} = J(\frac{\partial N}{\partial y}, T_a) \tag{51}$$

are the components of two vectors $\mathbf{q}^{\text{eff}} = (q^{eff}_1, q^{eff}_2)$, $\mathbf{q}^{gd} = (q^{gd}_1, q^{gd}_2)$, and $J(V,W) \equiv (\partial V/\partial x)(\partial W/\partial y) - (\partial W/\partial x)(\partial V/\partial y)$ is the Jacobian. Two non-dimensional number (E_1, E_2) are defined by

$$E_1 \equiv \frac{O\left(\left|q_1^{gd}\right|\right)}{O\left(\left|q_1^{eff}\right|\right)} = \frac{O\left(\left|J(\frac{\partial N}{\partial x}, T_a)\right|\right)}{O\left(\left|J(\frac{\partial Z}{\partial x}, T_a)\right|\right)}, \quad E_2 \equiv \frac{O\left(\left|q_2^{gd}\right|\right)}{O\left(q_2^{eff}\right)} = \frac{O\left(\left|J(\frac{\partial N}{\partial y}, T_a)\right|\right)}{O\left(\left|J(\frac{\partial Z}{\partial y}, T_a)\right|\right)} \tag{52}$$

to identify relative importance of gravity disturbance vector ($\delta\mathbf{g}$) versus the effective gravity ($\mathbf{g}_{\text{eff}}$) on the two components of the Q vector.

The NCEP/NCAR reanalyzed global long-term annual mean geopotential height (Z) and temperature (T_a) are used to calculate $|q^{eff}_1|$ at 1,000 hPa (Figure 12a), 850 hPa (Figure 12b), and 500 hPa (Figure 12c) and $|q^{eff}_2|$ at 1,000 hPa (Figure 13a), 850 hPa (Figure 13b), and 500 hPa (Figure 13c). The static gravity field model EIGEN-6C4 (for N) and NCEP/NCAR reanalyzed global long-term annual mean temperature (T_a) are used to calculate $|q^{gd}_1|$ at 1,000 hPa (Figure 12d), 850 hPa (Figure 12e), and 500 hPa (Figure 12f) and $|q^{gd}_2|$ at 1,000 hPa (Figure 13d), 850 hPa (Figure 13e), and 500 hPa (Figure 13f). The histograms of $|q^{eff}_1|$ show positively skewed distributions with the mean of 1.966×10^{-16}m^{-1} at 1,000 hPa (Figure 14a), 1.199×10^{-16}m^{-1} at 850 hPa (Figure 14b), and 0.4915×10^{-16}m^{-1} at 500 hPa (Figure 14c). The histograms of $|q^{gd}_1|$ show positively skewed distributions with the mean of 2.805×10^{-16}m^{-1} at 1,000 hPa (Figure 14d), 2.380×10^{-16}m^{-1} at 850 hPa (Figure 14e), and 1.649×10^{-16}m^{-1} at 500 hPa (Figure 14f). The E_1 number varies from 1.4268 (min) at 1,000 hPa to 4.3834 (max) at 100 hPa (Table 5). Similarly, the histograms of $|q^{eff}_2|$ show positively skewed distributions with the mean of 1.760×10^{-16}m^{-1} at 1,000 hPa (Figure 15a), 1.075×10^{-16}m^{-1} at 850 hPa (Figure 15b), and 0.4684×10^{-16}m^{-1} at 500 hPa (Figure 15c). The histograms

Preprints (www.preprints.org) | NOT PEER-REVIEWED | Posted: 7 February 2023 doi:10.20944/preprints202302.0127.v1

of $|q_2^{gd}|$ show positively skewed distributions with the mean of 0.9649×10^{-16}m^{-1} at 1,000 hPa (Figure 15d), 0.7790×10^{-16}m^{-1} at 850 hPa (Figure 15e), and 0.4720×10^{-16}m^{-1} at 500 hPa (Figure 15f). The E_2 number varies from 0.5482 (min) at 1,000 hPa to 1.057 (max) at 600 hPa (Table 6). It clearly demonstrates that the effect of $\delta\mathbf{g}$ is important in the Q vector.

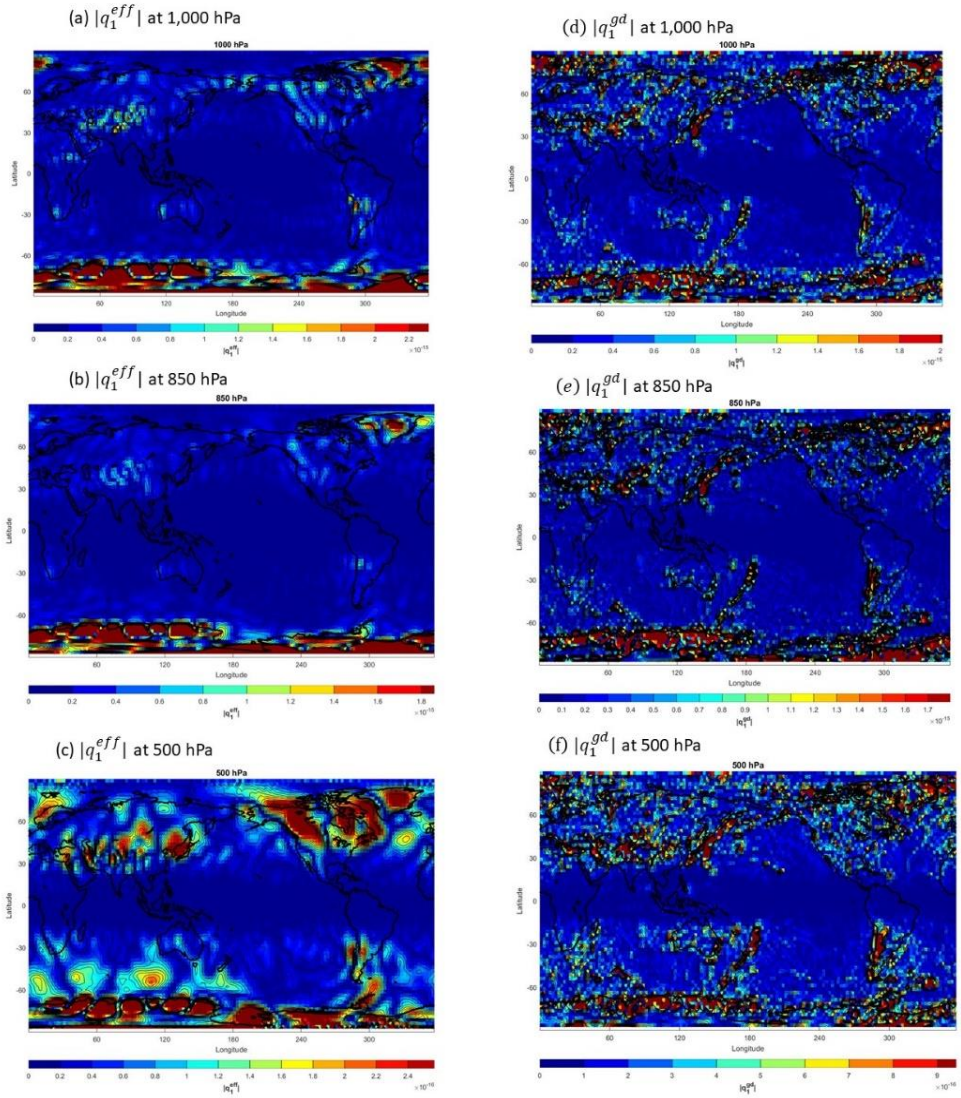

Figure 12. Horizontal distributions of $|q_1^{eff}|$ on (a) 1,000 hPa, (b) 850 hPa, (c) 500 hPa, and of $|q_1^{gd}|$ on (d) 1,000 hPa, (e) 850 hPa, and (f) 500 hPa.

Preprints (www.preprints.org) | NOT PEER-REVIEWED | Posted: 7 February 2023 doi:10.20944/preprints202302.0127.v1

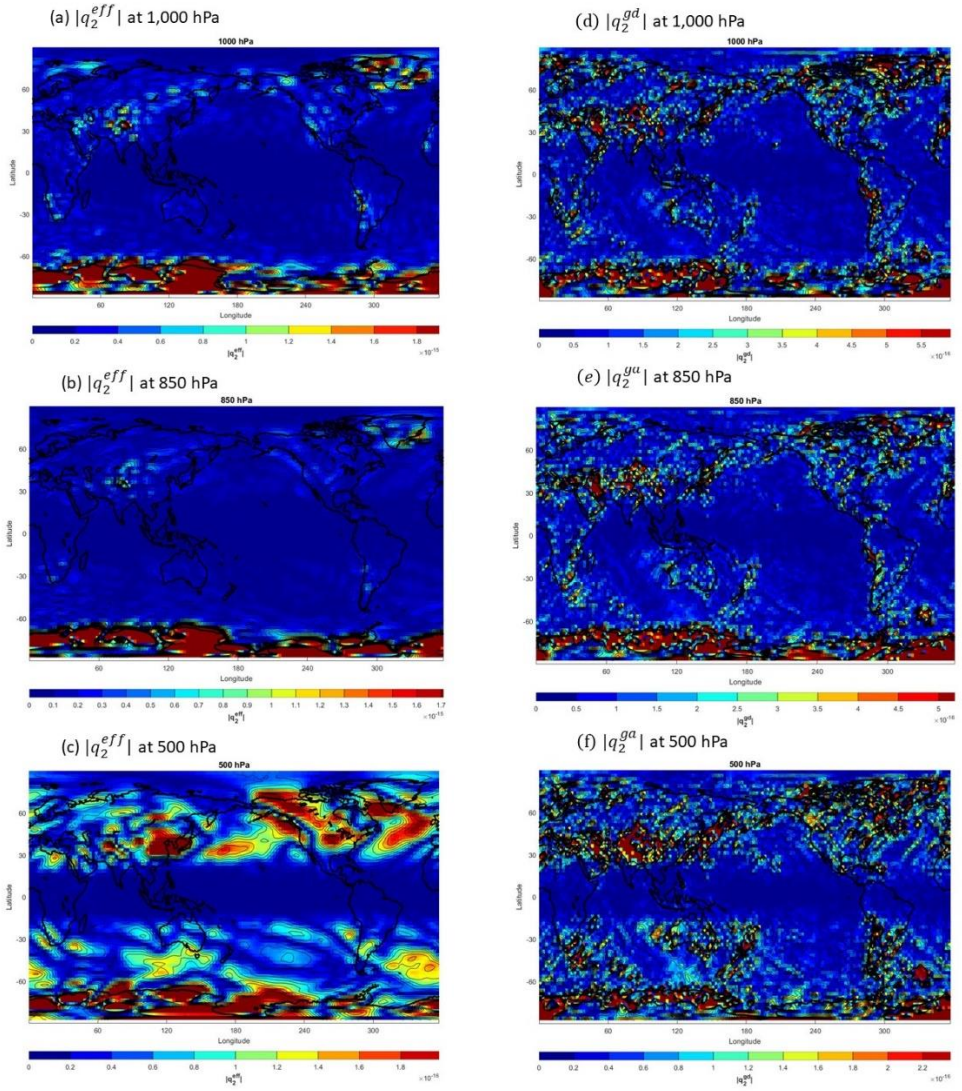

Figure 13. Horizontal distributions of $|q_2^{eff}|$ on (a) 1,000 hPa, (b) 850 hPa, (c) 500 hPa, and of $|q_2^{gd}|$ on (d) 1,000 hPa, (e) 850 hPa, and (f) 500 hPa.

Preprints (www.preprints.org) | NOT PEER-REVIEWED | Posted: 7 February 2023 doi:10.20944/preprints202302.0127.v1

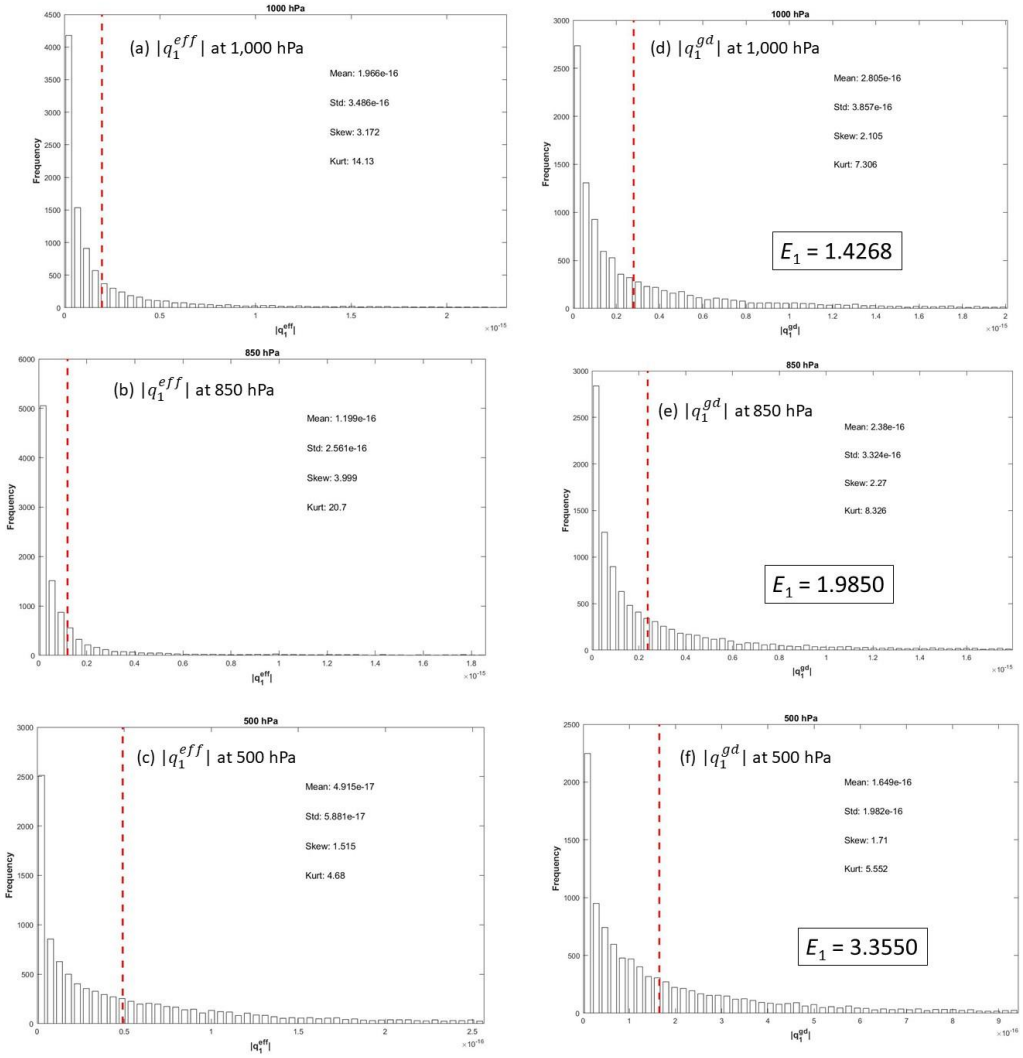

Figure 14. Histograms of $|q_1^{eff}|$ on (a) 1,000 hPa, (b) 850 hPa, (c) 500 hPa, and of $|q_1^{gd}|$ on (d) 1,000 hPa, (e) 850 hPa, and (f) 500 hPa with four statistical parameters (mean, standard deviation, skewness, kurtosis) and E_1 number on (d), (e), and (f). The red dashed lines show the mean values from the corresponding histograms.

Preprints (www.preprints.org) | NOT PEER-REVIEWED | Posted: 7 February 2023 doi:10.20944/preprints202302.0127.v1

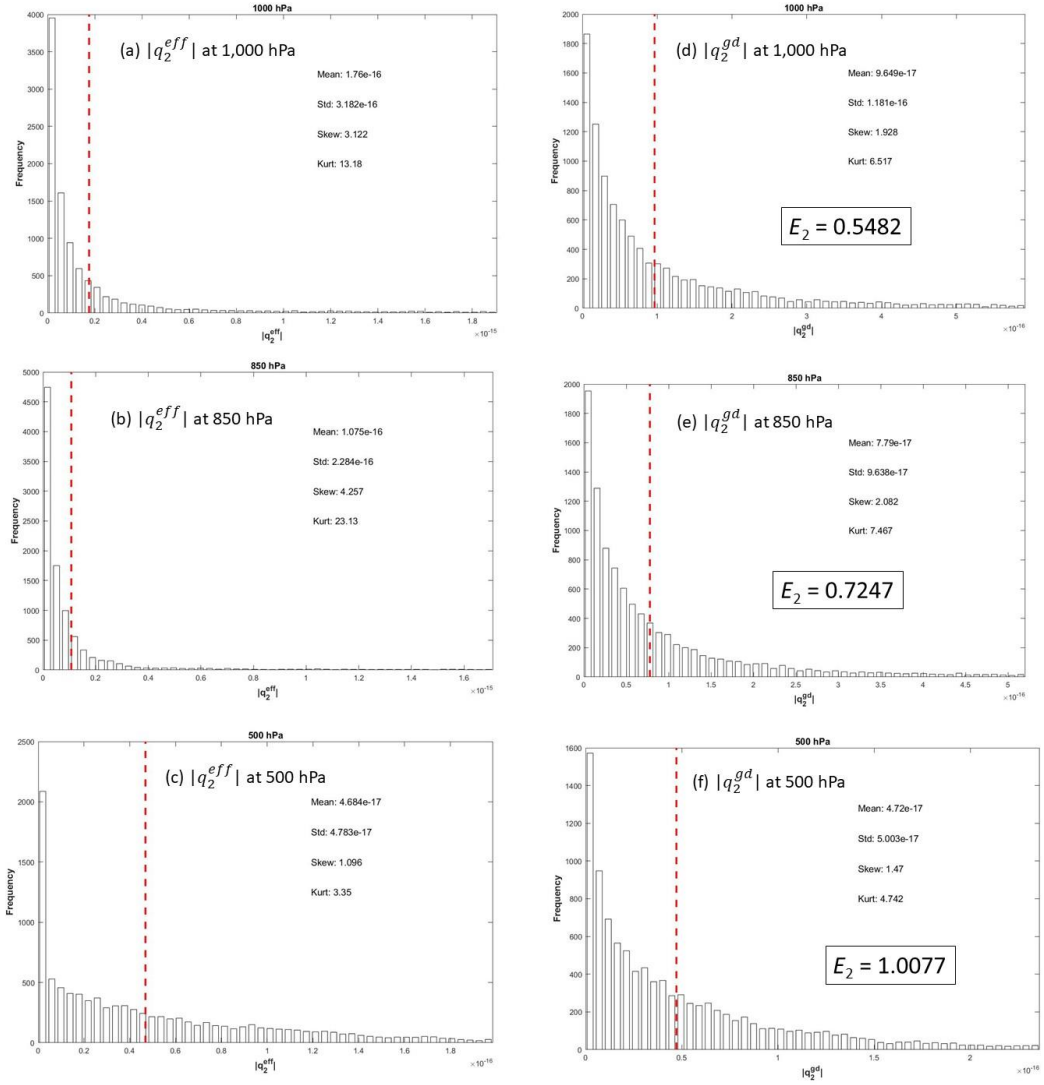

Figure 15. Histograms of $|q_2^{eff}|$ on (a) 1,000 hPa, (b) 850 hPa, (c) 500 hPa, and of $|q_2^{gd}|$ on (d) 1,000 hPa, (e) 850 hPa, and (f) 500 hPa with four statistical parameters (mean, standard deviation, skewness, kurtosis) and E_2 number on (d), (e), and (f). The red dashed lines show the mean values from the corresponding histograms.

Table 5. Global means of $|q_1^{gd}|$ and annual $|q_1^{eff}|$ at 12 pressure levels in the troposphere (treated as the order of magnitude) as well as the non-dimensional E_1-number.

Preprints (www.preprints.org) | NOT PEER-REVIEWED | Posted: 7 February 2023 doi:10.20944/preprints202302.0127.v1

Pressure Level (hPa)	Mean ($\lvert q_1^{eff} \rvert$) (10^{-16} m^{-1})	Mean ($\lvert q_1^{gd} \rvert$) (10^{-16} m^{-1})	E_1-number
1,000	1.966	2.805	1.4268
925	1.516	2.533	1.6708
850	1.199	2.380	1.9850
700	0.7411	2.121	2.8620
600	0.5468	1.814	3.3175
500	0.4915	1.649	3.3550
400	0.4553	1.508	3.3121
300	0.3765	1.130	3.0013
250	0.2813	0.9059	3.2204
200	0.2023	0.6462	3.1943
150	0.2630	0.9091	3.4567
100	0.3203	1.404	4.3834

Preprints (www.preprints.org) | NOT PEER-REVIEWED | Posted: 7 February 2023 doi:10.20944/preprints202302.0127.v1

Table 6. Global means of $|q_2^{gd}|$ and annual $|q_2^{eff}|$ at 12 pressure levels in the troposphere (treated as the order of magnitude) as well as the non-dimensional E_2-number.

Pressure Level (hPa)	Mean ($|q_2^{eff}|$) (10^{-16} m^{-1})	Mean ($|q_2^{gd}|$) (10^{-16} m^{-1})	E_2-number
1,000	1.760	0.9649	0.5482
925	1.381	0.8569	0.6205
850	1.075	0.7790	0.7247
700	0.6787	0.6174	0.9097
600	0.4948	0.5230	1.0570
500	0.4684	0.4720	1.0077
400	0.4614	0.4335	0.9395
300	0.4359	0.3527	0.8091
250	0.3704	0.2884	0.7786
200	0.3116	0.2128	0.6829
150	0.3628	0.2826	0.7789
100	0.4330	0.4315	0.9965

3.8. Omega equation

The quasi-geostrophic Omega equation on the *f*-plane given by [1] (P.170, Equation 6.53)

$$\sigma\nabla^2\omega + f^2\frac{\partial^2\omega}{\partial p^2} = -2\nabla\bullet\mathbf{Q} - \frac{\kappa}{p}\nabla^2 J$$

(53)

is used to diagnose the large-scale atmospheric vertical motion. Here, $\kappa = R/c_p$, c_p is the specific heat; and J is the rate of heating per unit mass due to radiation, conduction, and latent heat release. Substitution of (49) into (53) leads to

$$\sigma\nabla^2\omega + f^2\frac{\partial^2\omega}{\partial p^2} = -2\nabla\bullet\mathbf{Q}^{eff} - 2\nabla\bullet\mathbf{Q}^{gd} - \frac{\kappa}{p}\nabla^2 J \tag{54}$$

Substitution of (50) into (54) leads to

$$\nabla\bullet\mathbf{Q}^{eff} = \frac{R_a g_0}{pf}\nabla\bullet\mathbf{q}^{eff}, \quad \nabla\bullet\mathbf{Q}^{gd} = \frac{R_a g_0}{pf}\nabla\bullet\mathbf{q}^{gd} \tag{55}$$

Substitution of (51) into (55) gives

$$\nabla\bullet\mathbf{q}^{eff} = J(\nabla^2 Z, T_a) + J(\partial Z/\partial x, \partial T_a/\partial x) + J(\partial Z/\partial y, \partial T_a/\partial y) \tag{56}$$

$$\nabla\bullet\mathbf{q}^{gd} = J(\nabla^2 N, T_a) + J(\partial N/\partial x, \partial T_a/\partial x) + J(\partial N/\partial y, \partial T_a/\partial y) \tag{57}$$

A non-dimensional E_3 number is defined by

$$E_3 \equiv \frac{O\left(\left|\nabla\bullet\mathbf{Q}^{gd}\right|\right)}{O\left(\left|\nabla\bullet\mathbf{Q}^{eff}\right|\right)} = \frac{O\left(\left|\nabla\bullet\mathbf{q}^{gd}\right|\right)}{O\left(\left|\nabla\bullet\mathbf{q}^{eff}\right|\right)}$$

(58)

to identify relative importance of gravity disturbance vector ($\delta\mathbf{g}$) versus the effective gravity ($\mathbf{g}_{\text{eff}}$) on the Omega equation.

Preprints (www.preprints.org) | NOT PEER-REVIEWED | Posted: 7 February 2023 doi:10.20944/preprints202302.0127.v1

The NCEP/NCAR reanalyzed global long-term annual mean geopotential height (Z) and temperature (T_a) are used to calculate $|\nabla \bullet \mathbf{q}^{eff}|$ at 1,000 hPa (Figure 16a), 850 hPa (Figure 16b), and 500 hPa (Figure 16c). The static gravity field model EIGEN-6C4 (for N) and NCEP/NCAR reanalyzed global long-term annual mean temperature (T_a) are used to calculate $|\nabla \bullet \mathbf{q}^{gd}|$ at 1,000 hPa (Figure 16d), 850 hPa (Figure 16e), and 500 hPa (Figure 16f). The histograms of $|\nabla \bullet \mathbf{q}^{eff}|$ show positively skewed distributions with the mean of 6.603×10^{-22}m^{-1} at 1,000 hPa (Figure 17a), 3.142×10^{-22}m^{-1} at 850 hPa (Figure 17b), and 1.156×10^{-22}m^{-1} at 500 hPa (Figure 17c). The histograms of $|\nabla \bullet \mathbf{q}^{gd}|$ show positively skewed distributions with the mean of 17.06×10^{-22}m^{-1} at 1,000 hPa (Figure 17d), 14.17×10^{-22}m^{-1} at 850 hPa (Figure 17e), and 10.16×10^{-22}m^{-1} at 500 hPa (Figure 17f). The E_3 number varies from 2.584 (min) at 1,000 hPa to 11.713 (max) at 100 hPa (Table 7). It clearly demonstrates that the importance of $\delta\mathbf{g}$ in comparison to the effective gravity ($\mathbf{g}_{eff}$) in the Omega equation.

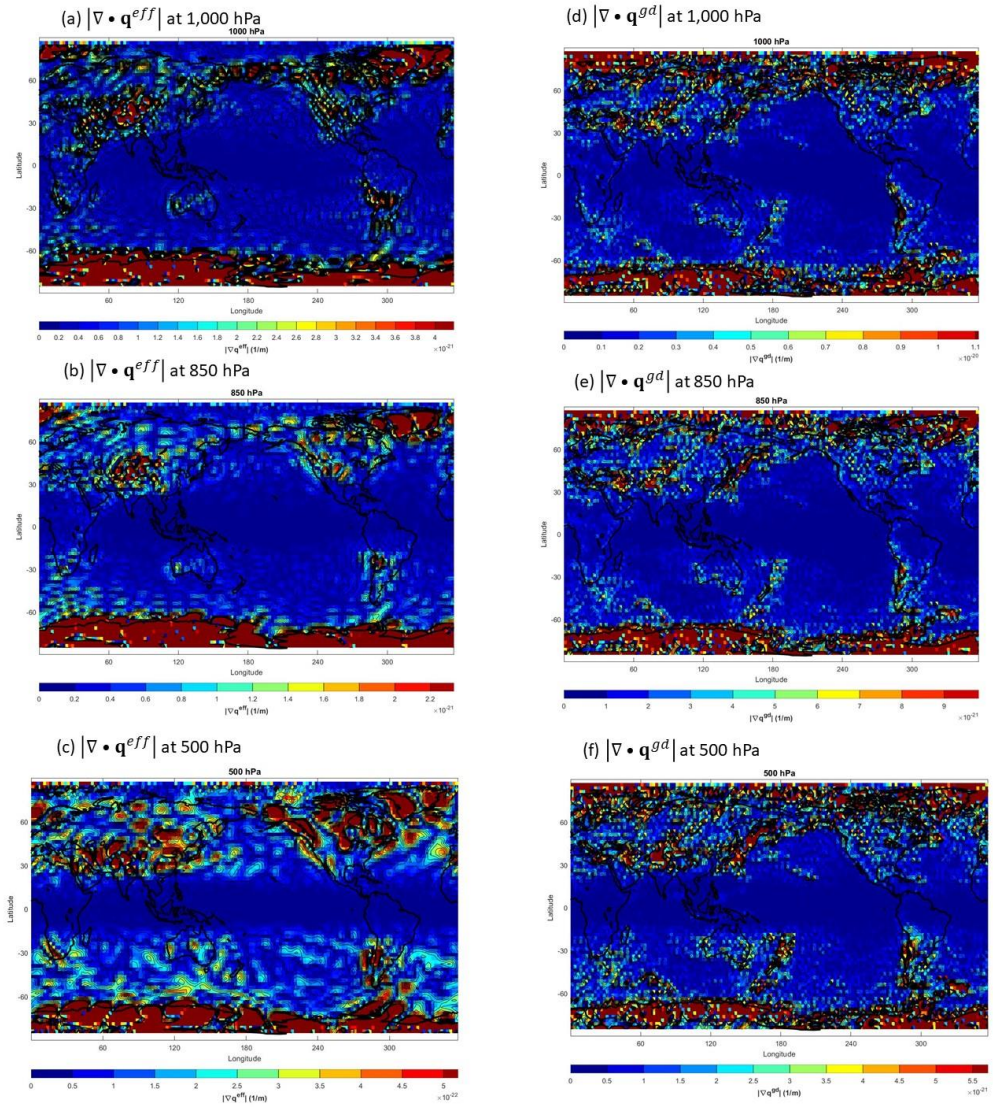

Figure 16. Horizontal distributions of $|\nabla \bullet \mathbf{q}^{eff}|$ on (a) 1,000 hPa, (b) 850 hPa, (c) 500 hPa, and of $|\nabla \bullet \mathbf{q}^{gd}|$ on (d) 1,000 hPa, (e) 850 hPa, and (f) 500 hPa.

Preprints (www.preprints.org) | NOT PEER-REVIEWED | Posted: 7 February 2023 doi:10.20944/preprints202302.0127.v1

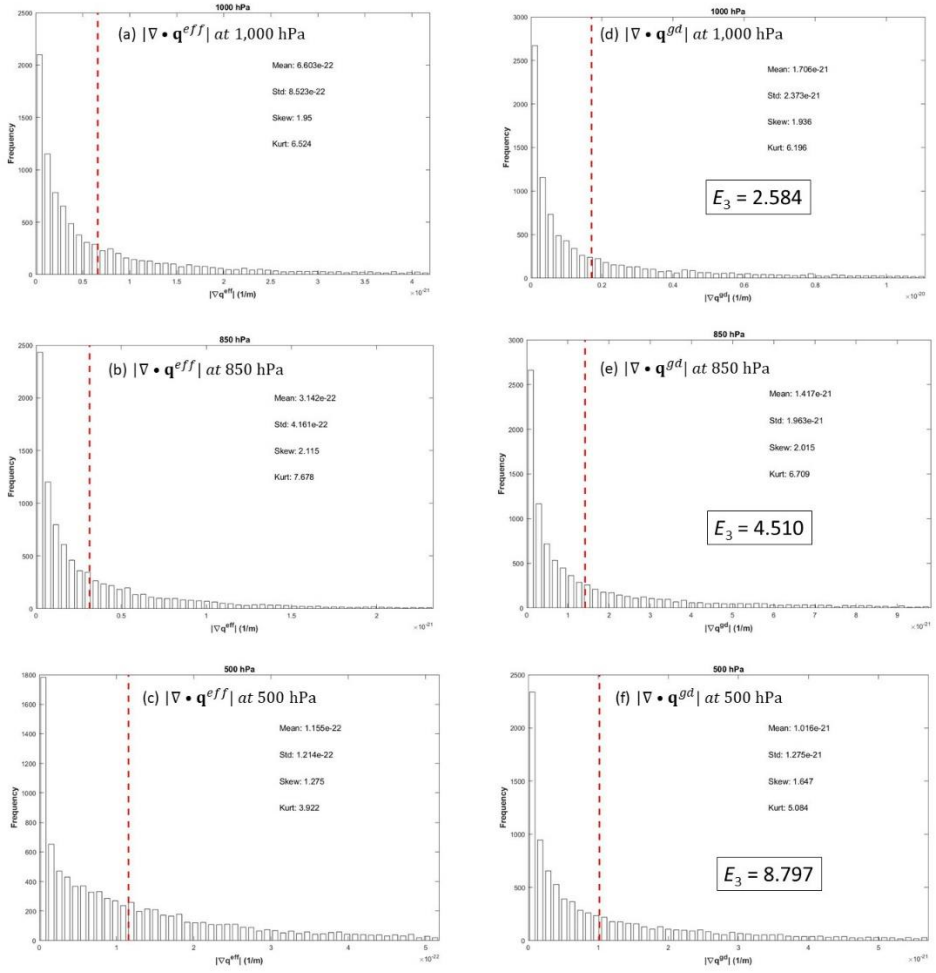

Figure 17. Histograms of $|\nabla \bullet \mathbf{q}^{eff}|$ on (a) 1,000 hPa, (b) 850 hPa, (c) 500 hPa, and of $|\nabla \bullet \mathbf{q}^{gd}|$ on (d) 1,000 hPa, (e) 850 hPa, and (f) 500 hPa with four statistical parameters (mean, standard deviation, skewness, kurtosis) and E_3 number on (d), (e), and (f). The red dashed lines show the mean values from the corresponding histograms.

Table 7. Global means of $|\nabla \bullet \mathbf{q}^{gd}|$ and annual $|\nabla \bullet \mathbf{q}^{eff}|$ at 12 pressure levels in the troposphere (treated as the order of magnitude) as well as the non-dimensional E_3-number.

Pressure Level (hPa)	Mean ($\|\nabla \bullet \mathbf{q}^{eff}\|$) ($10^{-22}$ m^{-1})	Mean ($\|\nabla \bullet \mathbf{q}^{gd}\|$) (10^{-22} m^{-1})	E_3-number
1,000	6.603	17.06	2.584
925	4.486	15.10	3.366
850	3.142	14.17	4.510
700	1.787	12.35	6.911
600	1.270	10.95	8.622
500	1.155	10.16	8.797
400	1.054	9.311	8.834
300	0.9258	6.939	7.495
250	0.7629	5.813	7.620
200	0.5760	4.416	7.667
150	0.6631	6.077	9.165
100	0.8011	9.383	11.713

Preprints (www.preprints.org) | NOT PEER-REVIEWED | Posted: 7 February 2023 doi:10.20944/preprints202302.0127.v1

4. Discussion

The effective gravity $\mathbf{g}_{eff}$ used in large-scale atmospheric dynamics and modeling is untrue since it is obtained from shrinking the Earth into a point-mass with entire mass concentrated at the Earth center. The true gravity $\mathbf{g}$ minus the effective gravity $\mathbf{g}_{eff}$ is the gravity disturbance vector $\delta\mathbf{g}$ ($\delta\mathbf{g} = \mathbf{g} - \mathbf{g}_{eff}$). The effect of $\delta\mathbf{g}$ in atmospheric dynamics is studied through replacing $\mathbf{g}_{eff}$ by $\mathbf{g}$. Seven non-dimensional numbers $(A, B, C, D, E_1, E_2, E_3)$ are defined to identify importance of horizontal component of $\delta\mathbf{g}$ versus the horizontal temperature gradient (A number), the pressure gradient force (B number), the Coriolis force (C number), the traditional geostrophic vorticity (D number), the components of traditional Q vector (E_1, E_2 numbers), and the components of traditional Omega equation (E_3 number).

Two reputable, independent, and openly available datasets (a) ICGEM EIGEN-6C4 and (b) NCEP/NCAR Reanalysis long term mean data are used to compute the seven numbers. Table 8 presents these numbers at 12 pressure levels in troposphere (1,000 – 100 hPa). Among them, only the A number is smaller than 0.0198×10^{-2} in the whole troposphere, which means that the effect of $\delta\mathbf{g}$ on the thermal wind relation is negligible. The B number varies from 0.4176 (max) at 850 hPa to 0.1630 (min) at 200 hPa with a mean of 0.2792 and the C number changes from 0.6168 (max) at 1,000 hPa to 0.1573 (min) at 200 hPa with a mean of 0.3052 in the troposphere. Both B and C numbers are greater than 0.27 for 1,000-500 hPa, and show that $\delta\mathbf{g}$ is non-negligible in comparison to $\mathbf{g}_{eff}$ in the geostrophic wind especially in lower troposphere (1,000-500 hPa). The D number varies from 1.3381 (max) at 500 hPa to 0.6712 (min) at 1,000 hPa with a mean of 1.0718, and shows that $\delta\mathbf{g}$ is comparable to $\mathbf{g}_{eff}$ in the geostrophic vorticity. The E_1 number varies from 4.3834 (max) at 100 hPa to 1.4268 (min) at 1,000 hPa with a mean of 2.9313 and the E_2 number changes from 1.0570 (max) at 600 hPa to 0.5482 (min) at 1,000 hPa with a mean of 0.8211. Both E_1 and E_2 numbers show that $\delta\mathbf{g}$ is comparable to $\mathbf{g}_{eff}$ in in the Q vector. The E_3 number varies from 11.713 (max) at 100 hPa to 2.584 (min) at 1,000 hPa with a mean of 7.271, and shows that $\delta\mathbf{g}$ is extremely important in comparison to $\mathbf{g}_{eff}$ in the Omega equation. In summary, the true gravity g should replace the effective gravity $\mathbf{g}_{eff}$, or the true geopotential ($\Phi = \Phi_{eff} - T$) should replace the effective geopotential (Φ_{eff}) in large-scale atmospheric dynamics and modeling.

Preprints (www.preprints.org) | NOT PEER-REVIEWED | Posted: 7 February 2023 doi:10.20944/preprints202302.0127.v1

Table 8. Non-dimensional A, B, C, D, E_1, E_2, E_3 numbers at 12 pressure levels in the troposphere (obtained from the 4th column of Tables 1-7) to represent the importance of gravity disturbance vector $\delta\mathbf{g}$ in large-scale atmospheric dynamics and modeling.

Pressure Level (hPa)	A Thermal Wind	B Geostrophic Wind	C Geostrophic Wind	D Geostrophic Vorticity/ Ekman Pumping	E_1 Q_1	E_2 Q_2	E_3 Omega Equation
1,000	0.0052	0.4052	0.6168	0.6712	1.4268	0.5482	2.584
925	0.0056	0.4151	0.5086	0.7539	1.6708	0.6205	3.366
850	0.0059	0.4176	0.4724	0.8534	1.9850	0.7247	4.510
700	0.0061	0.3836	0.3829	1.1078	2.8620	0.9097	6.911
600	0.0073	0.3435	0.3327	1.3344	3.3175	1.0570	8.622
500	0.0082	0.2849	0.2783	1.3381	3.3550	1.0077	8.797
400	0.0083	0.2298	0.2241	1.2529	3.3121	0.9395	8.834
300	0.0098	0.1861	0.1797	1.1169	3.0013	0.8091	7.495
250	0.0127	0.1713	0.1645	1.0701	3.2204	0.7786	7.590
200	0.0198	0.1630	0.1573	1.0564	3.1943	0.6829	7.667
150	0.0125	0.1639	0.1611	1.0955	3.4567	0.7789	9.165
100	0.0076	0.1869	0.1837	1.2109	4.3834	0.9965	11.713
Mean	0.0091	0.2792	0.3052	1.0718	2.9313	0.8211	7.271

 doi:10.20944/preprints202302.0127.v1

5. Conclusions

The Earth gravitation in atmosphere is currently identified through 'shrinking' the solid Earth into a point-mass with the entire Earth mass concentrated at the Earth center, and therefore it is not true and should be called the untrue Earth gravitation. The true Earth gravitation, according to the Newton's universal law of gravitation, is the volume integration of gravitation of all point-masses inside the Earth on a point-mass in atmosphere. Subtraction of the untrue Earth gravitation from the true Earth gravitation is the gravity disturbance vector $\delta\mathbf{g}$. With the Earth self-spinning, $\delta\mathbf{g}$ is also the subtraction of the effective gravity ($\mathbf{g}_{\text{eff}}$, currently used in atmospheric dynamics and modeling) from the true gravity ($\mathbf{g}$). This study shows the importance of $\delta\mathbf{g}$ in large-scale atmospheric dynamics such as geostrophic wind, geostrophic vorticity, Ekman pumping, Q-vector, and Omega equation, in comparison to the effective gravity ($\mathbf{g}_{\text{eff}}$), horizontal pressure gradient force, and Coriolis force, and in turn demonstrates the urgency to include $\delta\mathbf{g}$ (or to use the true gravity $\mathbf{g}$) in large-scale atmospheric modeling. Besides, it is easy to include $\delta\mathbf{g}$ in any atmospheric numerical models since $\delta\mathbf{g}$ has been quantitatively provided by geodetic community gravity field models.

Funding: This research received no external funding.

Institutional Review Board Statement: Not applicable.

Informed Consent Statement: Not applicable.

Data Availability Statement: The latest combined global gravity field model EIGEN-6C4 [$N(\lambda, \varphi)$, $T_z(\lambda, \varphi, 0)$] data is provided by the International Centre for Global Earth Models (ICGEM), Potsdam, Germany, from its website http://icgem.gfz-potsdam.de/home. The long-term annual mean (Z, u, v, T_a) data at 12 pressure levels 1,000, 925, 850, 700, 600, 500, 400, 300, 250, 200, 150, and 100 hPa is provided by the NOAA Physical Sciences Laboratory, Boulder, Colorado, USA, from its website https://psl.noaa.gov/data/gridded/data.ncep.reanalysis.derived.pressue.html.

Acknowledgments: The author would like to thank Mr. Chenwu Fan for computational assistance, the International Centre for Global Earth Models (ICGEM) for the EIGEN-6C4 [$N(\lambda, \varphi)$, $T_z(\lambda, \varphi, 0)$] data, and NCEP and NCAR for the long-term annual mean (Z, u, v, T_a) reanalyzed data at 12 pressure levels.

Conflicts of Interest: The author declares no conflict of interest.

Appendix A

References

1. Holton J.R. *An Introduction to Dynamic Meteorology*, 3rd ed.; Elsevier Academic Press: San Francisco, USA, 2004; pp. 1-535.
2. Gill, A. E. *Atmosphere-Ocean Dynamics*. Academic Press, 1st ed.; Academic Press: San Diego, USA, 1982; pp. 1-662.
3. Saniforth, A.; White, A. Geophysically realistic, ellipsoidal, analytically tractable (GREAT) coordinates for atmospheric and oceanic modeling. *Quart. J. Royal Meteorol. Soc.*, 2015, **141**, 1646-1657.
4. Vaníček, P., Krakiwsky, E. (1986). *Geodesy: the Concepts*, 2nd ed.; North-Holland; Amsterdam, Netherlands, 1986; p.72.
5. Wu, G.-X. 1984: The nonlinear response of the atmosphere to large-scale mechanical and thermal forcing. *J. Atmos. Sci.*, 1984, **41**, 2456-2476.
6. Stathopoulos, C., Galanis, G., Kallos, G. A coupled modeling study of mechanical and thermodynamical air-ocean interface processes under sea storm conditions. Dyn. Atmos. Oceans, 2020, **91**, 101140, https://doi.org/10.1016/j.dynatmoce.2020.101140
7. Chu, P.C. True gravity in ocean dynamics Part-1 Ekman transport. *Dyn. Atmos. Oceans*, 2021, **96**, 101268, doi.org/10.1016/j.dynatmoce.2021.101268
8. Shum, C.K., Tapley, B.D., Yuan, D.N., Ries, J.C., Schutz, B.E. An improved model for the Earth's gravity field. In Gravity, Gradiometry and Gravimetry, 1st ed.; Rummel, R., Hipkin, R.G., Eds.; Springer, New York, USA, 1990, 97-108.

9. Kostelecký, J., Klokočnìk, J., Bucha, B., Bezděk, A., and Förste, C. Evaluation of the gravity model EIGEN-6C4 in comparison with EGM2008 by means of various functions of the gravity potential and by BNSS/levelling. *Geoinformatics FCE CTU*, 2015, **14** (1), doi.org//10.14311/gi.14.1.1.
10. Sandwell, D.T., Smith, W.H.F. Marine gravity anomaly from Geosat and ERS 1 satellite altimetry. *J. Geophys.Res. – Solid Earth*, 1997, **102**, 10,039-10,054.
11. Gates, W.L. Derivation of the equations of atmospheric motion in oblate spherical coordinates. *J. Atmos. Sci.*, 2004, **61**, 2478-2487.
12. Beńard, P. An assessment of global forecast errors due to the spherical geopotential approximation in the shallow-water case. *Quart. J. Royal Meteorol. Soc.*, 2015, **141**, 195-206.